

Self-similar mixing in stratified plane Couette flow for varying Prandtl number

Qi Zhou^{1,†}, John R. Taylor¹ and Colm-cille P. Caulfield^{2,1}

¹Department of Applied Mathematics and Theoretical Physics, University of Cambridge, Wilberforce Road, Cambridge CB3 0WA, UK

²BP Institute, University of Cambridge, Madingley Road, Cambridge CB3 0EZ, UK

(Received xx; revised xx; accepted xx)

1 We investigate fully developed turbulence in stratified plane Couette flows using direct
 2 numerical simulations similar to those reported by Deusebio, Caulfield & Taylor (*J. Fluid*
 3 *Mech.*, 781, 2015) expanding the range of Prandtl number Pr examined by two orders
 4 of magnitude from 0.7 up to 70. Significant effects of Pr on the heat and momentum
 5 fluxes across the channel gap and on the mean temperature and velocity profile are
 6 observed. These effects can be described through a mixing length model coupling Monin–
 7 Obukhov (M-O) similarity theory and van Driest damping functions. We then employ
 8 M-O theory to formulate similarity scalings for various flow diagnostics for the stratified
 9 turbulence in the gap interior. The mid-channel-gap gradient Richardson number Ri_g is
 10 determined by the length scale ratio h/L , where h is the half channel gap depth and L
 11 is the Obukhov length scale. As h/L approaches very large values, Ri_g asymptotes to
 12 a maximum characteristic value of approximately 0.2. The buoyancy Reynolds number
 13 $Re_b \equiv \varepsilon/(\nu N^2)$, where ε is the dissipation, ν is the kinematic viscosity and N is the
 14 buoyancy frequency defined in terms of the local mean density gradient, scales linearly
 15 with the length scale ratio $L^+ \equiv L/\delta_\nu$, where δ_ν is the near-wall viscous scale. The
 16 flux Richardson number $Ri_f \equiv -B/P$, where B is the buoyancy flux and P is the
 17 shear production, is found to be proportional to Ri_g . This then leads to a turbulent
 18 Prandtl number $Pr_t \equiv \nu_t/\kappa_t$ of order unity, where ν_t and κ_t are the turbulent viscosity
 19 and diffusivity respectively, which is consistent with Reynolds analogy. The turbulent
 20 Froude number $Fr_h \equiv \varepsilon/(NU'^2)$, where U' is a turbulent horizontal velocity scale, is
 21 found to vary like $Ri_g^{-1/2}$. All these scalings are consistent with our numerical data
 22 and appear to be independent of Pr . The classical Osborn model based on turbulent
 23 kinetic energy balance in statistically stationary stratified sheared turbulence (*J. Phys.*
 24 *Oceanogr.*, 10, 1980), together with M-O scalings, results in a parameterization of $\kappa_t/\nu \sim$
 25 $\nu_t/\nu \sim Re_b Ri_g/(1 - Ri_g)$. With this parameterization validated through direct numerical
 26 simulation data, we provide physical interpretations of these results in the context of M-O
 27 similarity theory. These results are also discussed and rationalized with respect to other
 28 parameterizations in the literature. This paper demonstrates the role of M-O similarity
 29 in setting the mixing efficiency of equilibrated constant-flux layers, and the effects of
 30 Prandtl number on mixing in wall-bounded stratified turbulent flows.

31 **Key words:**

† Email address for correspondence: q.zhou@damtp.cam.ac.uk

1. Introduction

Stratified plane Couette flow is bounded by two horizontal walls moving in opposite directions with a constant velocity. The fluid density at each wall is held at a constant value with a lower density at the upper wall, resulting in a stably stratified system. Stratified plane Couette flow is one of several canonical geometries used to investigate the dynamics of stratified shear flows. Much of the research on stratified plane Couette flow has focused on transition and coherent structures (Deusebio *et al.* 2015; Eaves & Caulfield 2015), turbulent characteristics (García-Villalba *et al.* 2011*a*) and diapycnal mixing (Caulfield *et al.* 2004; Tang *et al.* 2009; García-Villalba *et al.* 2011*b*; Scotti 2015; Deusebio *et al.* 2015). In this paper, we consider the dynamical properties of turbulent stratified plane Couette flow. Our consideration has three main themes: (i) the effects of varying Prandtl number; (ii) the applicability of Monin–Obukhov similarity theory; and (iii) the parameterization of diapycnal mixing in stratified plane Couette flows. Each of the themes is associated with key open questions in the literature.

A stratified plane Couette flow can be characterised by three external parameters: the bulk Reynolds number Re ; the bulk Richardson number Ri ; and the Prandtl (Schmidt) number $Pr \equiv \nu/\kappa$ (or Sc), where κ is the scalar diffusivity and ν is the kinematic viscosity. While existing stratified plane Couette flow research spans a considerable range of Re and Ri , the Pr (or equivalently Sc) values examined have heretofore been limited to order unity. On the other hand, there has been growing evidence indicating that Pr (or Sc) can indeed have some first-order effects on stratified shear flows. For example, the effects of Pr on the characteristics of secondary instabilities and diapycnal mixing were reported by Salehipour *et al.* (2015) through simulations of growing Kelvin–Helmholtz instabilities. Motivated by these observations, we aim to investigate the effects of variations in Pr systematically in stratified plane Couette flows through direct numerical simulation (DNS), and this investigation constitutes the first theme of this paper.

Stratified plane Couette flows transfer momentum and heat fluxes across the upper and lower walls which provide shear and stratification to the system. In fully developed statistically stationary turbulent stratified plane Couette flows, which are the focus of the present study, the *total* momentum and active scalar fluxes are constant in the wall-normal (vertical) direction y . The very fact that these fluxes are constant in y contrasts stratified plane Couette flows with other wall-bounded flows, such as channel flows (Armenio & Sarkar 2002; García-Villalba & del Álamo 2011; Karimpour & Venayagamoorthy 2014, 2015), where the total momentum flux is maximised at the walls and zero at mid-channel (see e.g. Armenio & Sarkar (2002)). Turner (1973) argued that stably stratified flows may adjust to a tuned vertical flux from rearrangement of the mean flow and scalar profiles, and the turbulent characteristics in such generic constant-flux layers warrant further study.

For decades (see Foken (2006) for a review), the Monin–Obukhov similarity theory has provided a powerful tool to characterise such constant-flux layers. More recently, Monin–Obukhov theory has also been used to interpret stratified turbulence characteristics in homogeneous shear flows (Chung & Matheou 2012). In the context of stratified plane Couette flows, Deusebio *et al.* (2015) demonstrated the usefulness of Monin–Obukhov scaling by delineating the intermittency boundary in (Re, Ri) parameter space at a single Prandtl number $Pr = 0.7$. The Obukhov length scale

$$L \equiv \frac{u_\tau^3}{k_m g \alpha_V q_w}, \quad (1.1)$$

was found to be of dynamical significance in stratified plane Couette flows. Here, u_τ is

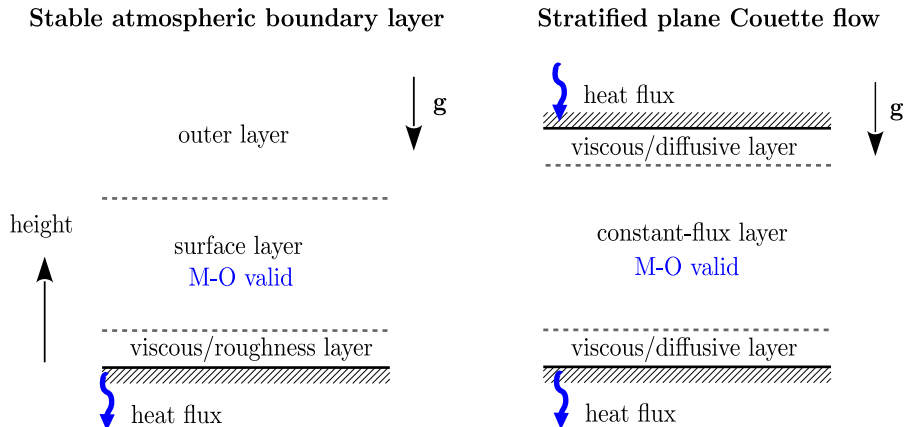


Figure 1: Comparison of a ‘weakly stable’ atmospheric boundary layer (see e.g. Mahrt (2014)) and a stratified plane Couette flow. The heights of various layers are not drawn to scale.

78 the friction velocity, k_m is the von Karman constant for momentum, g is gravity, α_V is
 79 the thermal expansion coefficient relating fluid temperature θ to density ρ via a linear
 80 equation of state

$$\rho = \rho_0(1 - \alpha_V\theta), \quad (1.2)$$

81 with ρ_0 being the reference density, and q_w is the wall heat flux. The ratio of length
 82 scales,

$$L^+ \equiv \frac{L}{\delta_\nu}, \quad (1.3)$$

83 where $\delta_\nu \equiv \nu/u_\tau$ is the near-wall viscous length scale, needs to be above approximately
 84 200 for a stratified plane Couette flow to stay fully turbulent, while when $L^+ < 200$
 85 the flows become intermittent, i.e. laminar and turbulent flow patches coexist. This
 86 observation is consistent with Flores & Riley (2011) who reported similar behaviour
 87 in stably stratified boundary layers. Consistent with the L^+ criterion, Deusebio *et al.*
 88 (2015) were not able to find fully developed turbulence (see their figure 18) in the SPC
 89 system for $Ri > 0.2$ even for Re up to 280000, as the flow inevitably relaminarises due to
 90 the strong buoyancy effects, although it is important to appreciate that the simulations
 91 had imposed periodicity in the streamwise and spanwise directions, and the extent of the
 92 computational domain may play a non-trivial role. Subsequently, Scotti & White (2016)
 93 also used Monin–Obukhov similarity theory to consider, among other issues, the mixing
 94 properties of stratified plane Couette flow, but they restricted their attention to five
 95 simulations at relatively low $Ri \leq 0.1$ for $14250 \leq Re \leq 55000$, using our conventions,
 96 and the single value of $Pr = 1$, and so did not consider the parameter regime where this
 97 intermittency at high Re for sufficiently high Ri appears to arise.

98 In this paper, we employ Monin–Obukhov similarity theory to formulate scalings for
 99 relevant stratified flow diagnostics in stratified plane Couette flows, which forms the
 100 second theme of the paper. It is important to contrast the behaviour of stratified plane
 101 Couette flows with the more geophysically realistic flow in a stable atmospheric boundary
 102 layer, where the flow is only wall-bounded from below. In stable atmospheric boundary
 103 layers, Monin–Obukhov theory is only valid for the ‘weakly stable’ regime in the surface

layer where the momentum and buoyancy fluxes do not vary with height, as shown in the left panel of figure 1. Monin–Obukhov theory does not apply, for example, in the overlying outer layer, or in the ‘very stable’ regime where the constant-flux surface layer does not exist (see e.g. Mahrt (2014)). However, in the doubly bounded set-up of stratified plane Couette flows, as shown in the right panel of figure 1, the momentum and buoyancy fluxes do not vary over height under the condition of statistical stationarity, and Monin–Obukhov theory is indeed expected to hold throughout the domain, crucially because the flow is wall-bounded above and below, and so there is a y -independent vertical flux through the domain.

One of the specific goals of the paper is to examine whether stratified plane Couette flow (or any stable constant-flux layer to which Monin–Obukhov scaling applies) supports the strongly stratified turbulence regime (Lilly 1983; Billant & Chomaz 2001; Brethouwer *et al.* 2007; Riley & Lindborg 2012), a regime which requires $Re_b \gg 1$ and $Fr_h \ll 1$, where Re_b is the buoyancy Reynolds number and Fr_h is the horizontal turbulent Froude number. Re_b and Fr_h are defined as

$$Re_b \equiv \frac{\varepsilon}{\nu N^2} \quad \text{and} \quad Fr_h \equiv \frac{U'}{N \ell_h}, \quad (1.4)$$

where ε is the dissipation rate, N is the buoyancy frequency, U' is a characteristic turbulent horizontal velocity, and ℓ_h is the horizontal integral scale of the turbulence. Such a strongly stratified regime can be reached numerically in homogeneous and stationary flows with body forcing (Brethouwer *et al.* 2007; de Bruyn Kops 2015), and in unforced nonstationary flows with specific initial conditions (Riley & de Bruyn Kops 2003; Diamessis *et al.* 2011; Zhou 2015; Maffioli & Davidson 2015). However, the existence of the strongly stratified regime has not been reported in wall-bounded stratified flows (García-Villalba *et al.* 2011a; García-Villalba & del Álamo 2011; Deusebio *et al.* 2015). Whether this regime is realizable in such flows is a key issue that we investigate in this paper. As demonstrated in Scotti & White (2016), Monin–Obukhov scaling allows the construction of an estimate for Re_b , and so for flows exhibiting Monin–Obukhov scaling there is a convenient theoretical approach to consider the realizability of the strongly stratified regime.

Diapycnal mixing in stratified flows is a focal point of research (see the reviews of Linden (1979); Fernando (1991); Peltier & Caulfield (2003); Ivey *et al.* (2008)). Existing parameterizations of the diapycnal diffusivity κ_t , when normalised by the molecular viscosity ν , often involve Re_b as a parameter (Shih *et al.* 2005; Bouffard & Boegman 2013), although it has been widely debated if Re_b is the *only* parameter of relevance. For example, the additional effects of Ri_g and Pr have been highlighted by laboratory and numerical studies (Barry *et al.* 2001; Mater & Venayagamoorthy 2014; Salehipour & Peltier 2015; Salehipour *et al.* 2015; Maffioli *et al.* 2016; Scotti & White 2016) in parameterizing κ_t , where Ri_g is the gradient Richardson number defined as

$$Ri_g \equiv \frac{N^2}{S^2}, \quad (1.5)$$

with S being an appropriate mean vertical shear. A recent study by Maffioli *et al.* (2016) proposed an alternative scaling based upon the turbulent Froude number Fr_h defined in (1.4). Stratified plane Couette flow is an effective test bed for these parameterizations, as the parameters (Re_b , Ri_g , Pr , Fr_h) can be varied readily by adjusting the external properties (such as wall velocity, density difference, viscosity, etc) in simulations of stratified plane Couette flow. The final theme of this paper is, therefore, to characterize the diapycnal mixing due to stratified turbulence in stratified plane Couette flow at as

148 large a range of Ri_g , Re_b and Pr as possible and to identify the relevant parameters in
 149 determining the turbulent diffusivities in such flows.

150 In summary, the three main aims of this paper and the corresponding open questions
 151 are as follows:

152 (i) *Prandtl number effects*. For given values of (Re, Ri) , how do the mean flow and
 153 temperature profiles depend on Pr ? How do the wall fluxes of momentum and heat
 154 depend on Pr ? How does the intermittency boundary in (Re, Ri) parameter space vary
 155 with Pr ?

156 (ii) *Similarity scaling*. How well does Monin–Obukhov theory characterise fully de-
 157 veloped stratified plane Couette flow? How do diagnosed quantities such as Ri_g , Re_b
 158 and Fr_h , arising as outputs of the simulations, relate to the wall fluxes? How do those
 159 diagnostics relate to each other? Is the strongly stratified regime accessible in stratified
 160 plane Couette flows?

161 (iii) *Mixing parameterization*. How should one parameterize the turbulent diffusivities
 162 in stratified plane Couette flows? Which of the possible parameters (Re_b, Ri_g, Pr, Fr_h)
 163 play a role in these flows? Are these parameters independent of each other?

164 To address these questions, the rest of the paper is structured as follows. In §2 we
 165 describe our numerical simulations of stratified plane Couette flows. In §3, we review
 166 Monin–Obukhov similarity theory and develop a mixing length model incorporating
 167 Monin–Obukhov theory at various Prandtl numbers and applying near-wall corrections
 168 (unlike the $Pr = 1$ model presented in Scotti & White (2016) not specifically focussed on
 169 stratified plane Couette flow), to predict the wall fluxes in stratified plane Couette flow
 170 as a function of external parameters (Re, Ri, Pr) . In §4 we present the Prandtl number
 171 effects in stratified plane Couette flows through the modification of the near-wall layer
 172 and thus the wall fluxes, and explore the implications of these effects for the intermittency
 173 boundary in the (Re, Ri) plane. In §5 we employ Monin–Obukhov similarity theory to
 174 characterize the turbulence in the channel gap interior and formulate scalings for various
 175 flow diagnostics. In §6 we develop parameterizations for turbulent diffusivities in the
 176 channel gap interior and discuss the results in the context of Monin–Obukhov scalings
 177 presented in §5 and existing parameterizations in the literature. In §7 we provide some
 178 concluding remarks.

179 2. Numerical simulations

180 In this section we describe DNS of stratified plane Couette flows considered in this
 181 paper. These simulations follow closely those of Deusebio *et al.* (2015) (hereinafter
 182 referred to as DCT). With a brief summary provided here, we refer the interested reader
 183 to DCT for further details on the formulation of the stratified plane Couette simulations.
 184 Full descriptions of the DNS algorithms can be found in Taylor (2008) and Bewley (2010).

185 Consider the velocity vector $\mathbf{u} = (u, v, w)$ in the coordinate system (x, y, z) , where x
 186 and z are the periodic (horizontal) directions and y the wall-normal (vertical) direction.
 187 Two non-slip solid walls, moving in opposite directions in the x -direction at velocity
 188 $\pm U_w$, are located at $y = \pm h$ respectively. The temperatures θ at the upper and lower
 189 walls are fixed at $\pm T_w$ respectively, resulting in a statically stable stratified system. We
 190 consider the incompressible Navier-Stokes equations under the Boussinesq approximation

191 with a linear equation of state as given in (1.2):

$$\frac{\partial \mathbf{u}}{\partial t} + \mathbf{u} \cdot \nabla \mathbf{u} = -\frac{\nabla p}{\rho_0} + \nu \nabla^2 \mathbf{u} - \alpha_V \theta \mathbf{g}, \quad (2.1a)$$

$$\frac{\partial \theta}{\partial t} + \mathbf{u} \cdot \nabla \theta = \kappa \nabla^2 \theta, \quad (2.1b)$$

$$\nabla \cdot \mathbf{u} = 0, \quad (2.1c)$$

192 where ν and κ are the kinematic viscosity and thermal diffusivity respectively, and $\mathbf{g} \equiv$
 193 $-g\mathbf{e}_y$ represents gravity. (It is important to remember that the vertical axis in which
 194 gravity acts is denoted by y as is conventional in engineering wall-bounded flow contexts,
 195 whereas in geophysical contexts this direction is often denoted by z .)

196 Stratified plane Couette flows are characterized by three external parameters:

$$Re \equiv \frac{U_w h}{\nu}, \quad Ri \equiv \frac{\alpha_V T_w g h}{U_w^2} \quad \text{and} \quad Pr \equiv \frac{\nu}{\kappa}. \quad (2.2)$$

197 We denote the mean velocity and temperature by

$$U \equiv \langle u \rangle \quad \text{and} \quad \Theta \equiv \langle \theta \rangle, \quad (2.3)$$

198 respectively, where $\langle \dots \rangle$ represents horizontal averages over the statistically homogeneous
 199 x - z plane. The friction velocity u_τ and temperature θ_τ are defined as

$$u_\tau^2 \equiv \frac{\tau_w}{\rho_0} = \nu \left| \frac{\partial U}{\partial y} \right|_{y=\pm h} \quad \text{and} \quad \theta_\tau \equiv \frac{q_w}{u_\tau} \quad (2.4)$$

200 respectively, where $\tau_w \equiv \rho_0 u_\tau^2$ is the wall shear stress and

$$q_w \equiv \kappa \left| \frac{\partial \Theta}{\partial y} \right|_{y=\pm h} \quad (2.5)$$

201 is the wall heat flux. The Obukhov length scale L , defined in (1.1), is the only (up to
 202 a multiplicative constant) length scale that can be formed using u_τ^2 and q_w , the wall
 203 momentum and heat fluxes, along with the buoyancy parameter $g\alpha_V$, where α_V relates
 204 temperature to buoyancy via the linear equation of state (1.2). The friction velocity u_τ
 205 can be used to form the friction Reynolds number

$$Re_\tau \equiv \frac{u_\tau h}{\nu}, \quad (2.6)$$

206 and q_w can be made dimensionless to form the Nusselt number

$$Nu \equiv \frac{q_w h}{\kappa T_w} = \frac{h}{T_w} \left| \frac{\partial \Theta}{\partial y} \right|_{y=\pm h}. \quad (2.7)$$

207 Re_τ and Nu are not known *a priori*, but are rather output parameters which vary with
 208 the external parameters (Re , Ri , Pr).

209 In order to investigate the flow properties as the external parameters vary in the
 210 three-dimensional parameter space (Re , Ri , Pr), we first revisit the existing simulations
 211 performed by DCT who focused on a fixed $Pr = 0.7$ and varied Re and Ri extensively.
 212 A set of simulations performed by DCT at a wide range of Re from 865 to 280000 are
 213 reanalysed in the present study, and the parameters covered are listed in Table 1. In
 214 addition, new simulations are performed at a fixed Reynolds number $Re = 4250$ for
 215 various Pr and Ri . The Re value in the new simulations is large enough to support
 216 fully developed turbulence at finite values of Ri , (i.e. there is no observed spatial or

217 temporal intermittency in the turbulent flow in this geometry) and yet the Re value is
 218 small enough to allow, within available computing resources, a parametric study in the
 219 (Re, Pr) parameter space through DNS, which is one of the main aims of this paper.

220 The input and output parameters of these simulations, both newly performed (simula-
 221 tions 1–12) and reanalysed from the work of DCT (simulations 13–23), are tabulated in
 222 Table 1. Pr values spanning two orders of magnitude, i.e. $Pr \in \{0.7, 7, 70\}$, are considered
 223 in this paper. The choices of the first two Pr values correspond to the geophysically
 224 relevant scenarios of heat (as the active scalar) in air ($Pr = 0.7$) and heat in water
 225 ($Pr = 7$) respectively. While the direct geophysical relevance the third examined value
 226 of $Pr = 70$ is not immediately apparent, it has been chosen as an intermediate value
 227 between 7 and 700, the latter of which corresponds to the relevant Schmidt number Sc
 228 of salt in water. Simulation of flows with $Sc = 700$ incurs prohibitive computational
 229 costs presently. The $Pr = 70$ simulations are examined in an attempt to probe into the
 230 extremely poorly conductive/diffusive regime expected to occur for $Sc = 700$.

231 In addition to the requirements to resolve the near-wall dynamics adequately, which
 232 was described by DCT, the elevated Pr values pose their own requirement on the spatial
 233 resolution of the DNS, i.e. to resolve adequately the Batchelor scale of the scalar field ℓ_B
 234 (Batchelor 1959), where ℓ_B is defined as

$$\ell_B \equiv \frac{\eta}{Pr^{1/2}}, \quad (2.8)$$

235 and $\eta \equiv (\nu^3/\varepsilon)^{1/4}$ is the Kolmogorov scale. Equation (2.8) suggests that the grid resolu-
 236 tion needs to be approximately tripled when Pr is increased by one order of magnitude,
 237 given a fixed η . In setting up our simulations, simulation 3 (which is replicated from
 238 DCT's simulation 9 as tabulated in their table 1) with $(Re, Ri, Pr) = (4250, 0.04, 0.7)$, is
 239 used as a reference. When Pr is increased from 0.7 (as in DCT's simulations) to 7 (as in
 240 our simulations 4–8), the resolution is only doubled. However, grid-independence tests at
 241 $Pr = 7$ employing a $384 \times 193 \times 384$ grid yield no significant differences in the turbulence
 242 statistics, suggesting that the resolutions of our $Pr = 7$ simulations are sufficient. When
 243 Pr is increased from 7 to 70 in simulations 9–12, the resolution is tripled, as required by
 244 (2.8).

245 In stratified plane Couette flow simulations, the size of the computational domain
 246 may affect the results when the flow is intermittent, as suggested by DCT. All but
 247 one of the new simulations (1–12) performed have horizontal domain dimensions of
 248 $(L_x, L_z) = (4\pi h, 2\pi h)$, following the baseline cases adopted by DCT (i.e. simulations
 249 16–22). Due to the constraint of computational resources, however, the simulation of
 250 $(Re, Pr) = (0.04, 70)$ (simulation 9) is performed with the domain dimensions in x and
 251 z reduced to 50% of the other simulations, while keeping the same spatial resolution.
 252 As reported by DCT, the turbulence statistics are not expected to be sensitive to the
 253 domain size if the flow is fully turbulent, which is the case of simulation 9. Throughout
 254 this paper, we focus on examining the turbulence characteristics during the statistically
 255 stationary phase of the simulations where key statistics such as dU/dy , $d\Theta/dy$ and ε are
 256 observed to have reached a steady state. The spatially averaged statistics may fluctuate
 257 weakly with time (see DCT's figure 2(b) for example), and the statistics reported in
 258 the following are also time-averaged over a time scale of no shorter than $5h/U_w$, i.e. five
 259 advective time units, for the simulations with $Pr = 70$. For the simulations with $Pr = 0.7$
 260 and 7, the time-averaging window is typically longer than $50h/U_w$.

Run	Re	Pr	Ri	$(L_x, L_y, L_z)/h$	(N_x, N_y, N_z)	Re_τ	Nu	L^+
1	4250	0.7	0	$(4\pi, 2, 2\pi)$	(256, 129, 256)	233	10.6	∞
2	4250	0.7	0.01	$(4\pi, 2, 2\pi)$	(256, 129, 256)	215	9.26	2180
3	4250	0.7	0.04	$(4\pi, 2, 2\pi)$	(256, 129, 256)	181	6.40	394
4	4250	7	0	$(4\pi, 2, 2\pi)$	(512, 257, 512)	233	31.8	∞
5	4250	7	0.01	$(4\pi, 2, 2\pi)$	(512, 257, 512)	221	29.7	7660
6	4250	7	0.04	$(4\pi, 2, 2\pi)$	(512, 257, 512)	206	25.9	1640
7	4250	7	0.08	$(4\pi, 2, 2\pi)$	(512, 257, 512)	180	19.0	653
8	4250	7	0.12	$(4\pi, 2, 2\pi)$	(512, 257, 512)	129	8.47	261
9	4250	70	0.04	$(2\pi, 2, \pi)$	(768, 769, 768)	231	69.3	9590
10	4250	70	0.16	$(4\pi, 2, 2\pi)$	(1536, 769, 1536)	204	50.2	2020
11	4250	70	0.96	$(4\pi, 2, 2\pi)$	(1536, 769, 1536)	145	17.0	259
12	4250	70	1.44	$(4\pi, 2, 2\pi)$	(1536, 769, 1536)	107	11.2	78.0
13	865	0.7	0.02	$(64\pi, 2, 32\pi)$	(1024, 65, 1024)	47	2.17	256
14	2130	0.7	0.04	$(32\pi, 2, 16\pi)$	(1024, 97, 1024)	85	2.89	170
15	3925	0.7	0.06	$(16\pi, 2, 8\pi)$	(768, 129, 768)	130	3.56	148
16	12650	0.7	0.08	$(4\pi, 2, 2\pi)$	(512, 161, 512)	349	7.95	249
17	15000	0.7	0.05	$(4\pi, 2, 2\pi)$	(768, 257, 768)	497	13.9	666
18	15000	0.7	0.1	$(4\pi, 2, 2\pi)$	(512, 193, 512)	318	5.46	142
19	15600	0.7	0.1	$(4\pi, 2, 2\pi)$	(512, 193, 512)	335	5.81	152
20	25000	0.7	0.05	$(4\pi, 2, 2\pi)$	(768, 385, 768)	764	20.0	930
21	25000	0.7	0.1	$(4\pi, 2, 2\pi)$	(768, 257, 768)	520	8.80	227
22	35000	0.7	0.125	$(4\pi, 2, 2\pi)$	(768, 289, 768)	520	6.08	134
23	280000	0.7	0.175	$(2.66, 2, 1.33)$	(512, 513, 512)	1578	6.59	117

Table 1: Summary of numerical simulations of stratified plane Couette flows. Simulations 1–12 are performed specifically for the present study with a fixed $Re = 4250$ and varying Pr and Ri , and simulations 13–23 were first reported by Deusebio *et al.* (2015) with a fixed $Pr = 0.7$ and varying Re and Ri . The computational domains are of dimensions (L_x, L_y, L_z) , and the number of grid points in each direction is (N_x, N_y, N_z) respectively.

3. First-order closure model

Key quantities in describing stratified plane Couette flows in the framework of Monin–Obukhov similarity theory are the momentum flux u_τ^2 and wall heat flux q_w which are directly linked to the wall gradients via (2.4) and (2.5). It is thus desirable to develop a model to predict the fluxes for varying external parameters. DCT proposed such a model applying Monin–Obukhov theory to the Reynolds-averaged Navier-Stokes equations. However, the model only applied to a single Prandtl number ($Pr = 0.7$). A refined version of the model, which now uses a mixing length formulation to provide a first-order closure for the turbulent fluxes as a function of mean local gradients, is described here. The mixing length specifications are consistent with Monin–Obukhov theory, and near-wall corrections through damping functions (van Driest 1956; Pope 2000) ensure the reliable presentation of the effects of Pr on the wall fluxes.

3.1. Model formulation

In order to obtain the vertical profiles of mean velocity and temperature in fully developed turbulent stratified plane Couette flow, we integrate the following set of equations of U and Θ in time (using the laminar profiles as initial conditions) until reaching a steady state:

$$\frac{\partial U}{\partial t} = \nu \frac{\partial^2 U}{\partial y^2} + \frac{\partial}{\partial y} \left(\nu_t \frac{\partial U}{\partial y} \right), \quad (3.1)$$

$$\frac{\partial \Theta}{\partial t} = \kappa \frac{\partial^2 \Theta}{\partial y^2} + \frac{\partial}{\partial y} \left(\kappa_t \frac{\partial \Theta}{\partial y} \right), \quad (3.2)$$

where ν_t and κ_t are the turbulent (eddy) viscosity and diffusivity respectively.

The closure for ν_t in the Reynolds-averaged momentum equation (3.1) can be obtained by specifying a mixing length (see e.g. Pope (2000)):

$$\nu_t = \ell_m^{*2} \left| \frac{\partial U}{\partial y} \right| = \ell_m^* u^*, \quad (3.3)$$

where ℓ_m^* is the mixing length for momentum and the fluctuation velocity

$$u^* = \ell_m^* \left| \frac{\partial U}{\partial y} \right|. \quad (3.4)$$

Similarly, the turbulent flux of scalar in (3.2) can be modelled as

$$-\langle v'\theta' \rangle = \kappa_t \frac{\partial \Theta}{\partial y} = u^* \theta^* = \ell_m^* \left| \frac{\partial U}{\partial y} \right| \ell_s^* \frac{\partial \Theta}{\partial y}, \quad (3.5)$$

where ℓ_s^* is the scalar mixing length, and it follows that

$$\kappa_t = \ell_s^* \ell_m^* \left| \frac{\partial U}{\partial y} \right| = \ell_s^* u^*. \quad (3.6)$$

It remains to specify the two mixing lengths ℓ_m^* and ℓ_s^* .

To do this, we start by considering unstratified flows, i.e. $L \rightarrow \infty$. We define y_w as the wall-normal (vertical) distance to the closer wall, i.e. $y_w \equiv \min(h - y, h + y)$. The length y_w can be normalised in wall units as $y^+ \equiv y_w / (\nu / u_\tau)$. The ‘law of the wall’ of unstratified wall-bounded flows (see e.g. Bradshaw & Huang (1995)) prescribes the wall-normal gradients of U and Θ in the log-law region, i.e. $y^+ > 30$ (Pope 2000), as

$$\frac{\partial U}{\partial y} = \frac{u_\tau}{k_m y_w} \quad \text{and} \quad \frac{\partial \Theta}{\partial y} = \frac{\theta_\tau}{k_s y_w} = \frac{\theta_\tau \hat{P}r_t}{k_m y_w}. \quad (3.7)$$

where k_m and k_s are the von Karman constants for momentum and scalar respectively, and $\hat{P}r_t = k_m / k_s$ is a turbulent Prandtl number which applies for the log-law region.

With

$$u_\tau^2 \cong \nu_t \left| \frac{\partial U}{\partial y} \right| \quad \text{and} \quad q_w = \theta_\tau u_\tau \cong \kappa_t \left| \frac{\partial \Theta}{\partial y} \right|, \quad (3.8)$$

in the log-law region and following the model prescriptions in (3.3) and (3.6), the mixing lengths ℓ_m^* and ℓ_s^* corresponding to (3.7) read

$$\ell_m^* = k_m y_w \quad \text{and} \quad \ell_s^* = k_s y_w = \ell_m^* \hat{P}r_t^{-1}. \quad (3.9)$$

As a result, the velocity scale u^* in (3.3) and (3.6) can be specified as

$$u^* = u_\tau. \quad (3.10)$$

297 When the fluid is stratified, Monin–Obukhov similarity theory prescribes the vertical
298 gradients of U and Θ as

$$\frac{\partial U}{\partial y} = \frac{u_\tau}{k_m y_w} \Phi_m(\xi) \quad \text{and} \quad \frac{\partial \Theta}{\partial y} = \frac{\theta_\tau}{k_s y_w} \Phi_s(\xi). \quad (3.11)$$

299 In these expressions, Φ_m and Φ_s are Monin–Obukhov functions which are linear in the
300 non-dimensional variable $\xi \equiv y_w/L$ for stable stratification:

$$\Phi_m(\xi) = 1 + \beta_m \xi \quad \text{and} \quad \Phi_s(\xi) = 1 + \beta_s \xi. \quad (3.12)$$

301 Here we take $k_m = 0.41$ and $k_s = 0.48$ following Bradshaw & Huang (1995). The choice of
302 $\beta_m = 4.8$ follows the recommendation of Wyngaard (2010) and $\beta_s = 5.6$ is used following
303 the specific choice of k_m and k_s . These model constants are determined empirically using
304 field observations of stable atmospheric boundary layers, and their values can exhibit
305 some uncertainties (see Foken (2006) for a review). The form of the similarity functions
306 may also require additional corrections in order to match the field situations (see e.g.
307 Tastula *et al.* (2015)), such as varying fluxes with height. In the idealised situation
308 considered here, where the entire flow between the walls is a constant-flux layer by
309 construction, we use the classical canonical forms of Monin–Obukhov functions described
310 in (3.12) for clarity and simplicity.

311 The mixing length formulation corresponding to Monin–Obukhov theory becomes

$$\ell_m^* = k_m y_w \Phi_m^{-1}(\xi) \quad \text{and} \quad \ell_s^* = k_s y_w \Phi_s^{-1}(\xi). \quad (3.13)$$

312 Taking $\xi \rightarrow 0$ in (3.13), one recovers the unstratified formulation (3.9). Since ℓ_m^* and ℓ_s^*
313 are specified in (3.13) in very similar ways, the ratio ℓ_m^*/ℓ_s^* is expected to be of order
314 unity.

3.2. The near-wall layer

315 Here we focus on the viscous wall region, i.e. $y^+ < 50$ (Pope 2000), where the
316 (molecular) Prandtl number Pr plays a critical role. The mean velocity and temperature
317 differences relative to the closer wall can be written in wall units as

$$U^+ = \frac{\min(U + U_w, U_w - U)}{u_\tau} \quad \text{and} \quad \Theta^+ = \frac{\min(\Theta + T_w, T_w - \Theta)}{\theta_\tau}, \quad (3.14)$$

319 where the velocity and temperature at the upper and lower walls are fixed at $\pm U_w$ and
320 $\pm T_w$, respectively. In the viscous/conductive sublayer near the wall (as shown in figure
321 2 for Θ^+),

$$U^+ = y^+ \quad \text{and} \quad \Theta^+ = y^+ Pr. \quad (3.15)$$

322 As y^+ increases, the viscous/conductive sublayer transitions into the log-law region for
323 which the mean profiles can be obtained by integrating (3.7) to yield

$$U^+ = \frac{1}{k_m} \ln y^+ + C_m \quad \text{and} \quad \Theta^+ = \frac{1}{k_s} \ln y^+ + C_s = \frac{\hat{Pr}_t}{k_m} \ln y^+ + C_s. \quad (3.16)$$

324 DNS of stratified plane Couette flows recover such behaviour in the near-wall region, as
325 shown in figure 2. Unlike C_m which is a constant (we take $C_m = 5.0$ following Bradshaw
326 & Huang (1995)), C_s is thought to be a function of Pr , e.g. following Schlichting &
327 Gersten (2003),

$$C_s = 13.7 Pr^{2/3} - 7.5, \quad (3.17)$$

328 or following Davidson (2004),

$$C_s = 1.67(3Pr^{1/3} - 1)^2. \quad (3.18)$$

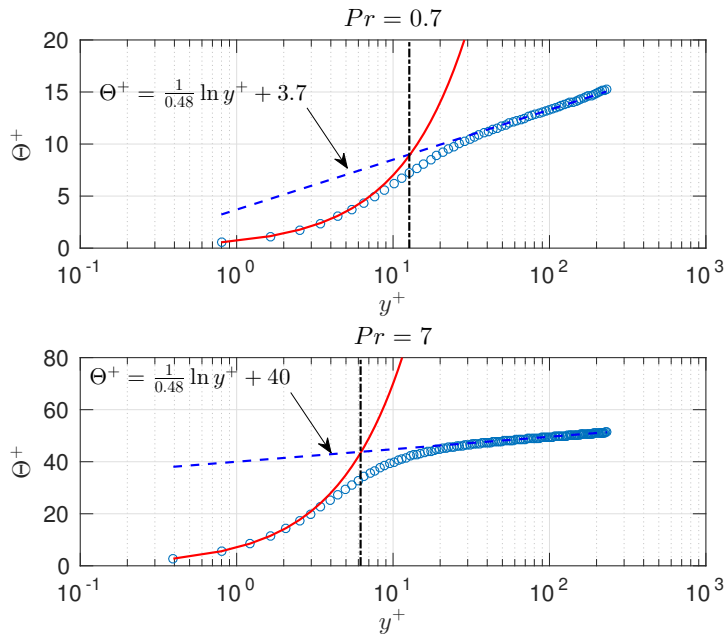


Figure 2: Normalized temperature difference from the wall value, Θ^+ as defined in (3.14), plotted as a function of normalized wall distance y^+ . Upper panel: $Pr = 0.7, Ri = 0$ (simulation 1); lower panel: $Pr = 7, Ri = 0$ (simulation 4). Circles show DNS data; the conductive law (3.15) is plotted with a solid line; the logarithmic law (3.16) in which the additive constant C_s varies with Pr , is plotted with a dashed line; and the dot-dashed line shows the location of $y^+ = \Delta y^+$, where Δy^+ marks the characteristic height of the conductive sublayer as defined in (3.19).

329 Figure 2 confirms such an effect of Pr on the log-law layer. The empirical estimates of
 330 C_s as a function of Pr , i.e. (3.17) and (3.18), agree well with DNS, as shown in figure 3.

331 The value of C_s effectively determines the height of the conductive sublayer which can
 332 be measured by Δy^+ (as marked with vertical dot-dashed lines in figure 2), the intersect
 333 of the conductive law (3.15) and the log law (3.16), i.e.

$$\Delta y^+ Pr = \frac{1}{k_s} \ln \Delta y^+ + C_s(Pr). \quad (3.19)$$

334 The quantity Δy^+ is observed to decrease with Pr (see figures 2 and 3), and, in particular,
 335 for $Pr \gg 1$ (Davidson 2004),

$$\Delta y^+ \propto Pr^{-1/3}. \quad (3.20)$$

336 With (3.15), the temperature difference across the conductive sublayer, i.e.

$$\Delta \Theta^+ \sim Pr \Delta y^+ \propto Pr^{2/3}, \quad (3.21)$$

337 varies strongly with Pr .

338 It is thus shown that Pr has a significant effect on the near-wall structure of the mean
 339 scalar field. A thinner conductive layer is expected at higher values of Pr , as suggested by
 340 (3.20). Moreover, as the temperature gradients (in wall units) are sharper at a larger Pr ,
 341 as quantified by (3.15), the temperature jump across the conductive sublayer increases
 342 with Pr , as quantified by (3.21). This generic behaviour of the ‘law of the wall’ for varying

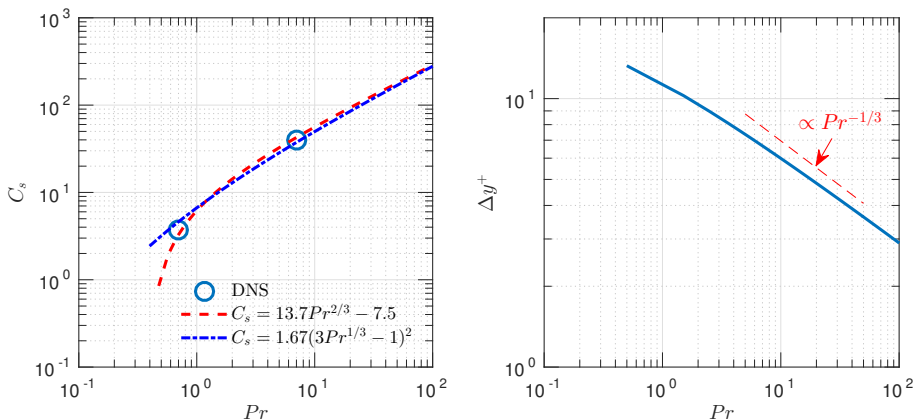


Figure 3: Effect of Pr on the near-wall layer. Left panel: Variation with Pr of the additive constant C_s in the log law for scalar (3.16) as determined by simulations 1 and 4 of stratified plane Couette flows and empirical relations (3.17) and (3.18). Right panel: The height of the conductive sublayer Δy^+ as a function of Pr . Δy^+ values obtained by solving (3.19) and (3.17) are plotted with a solid line, while the dashed line shows the scaling $\Delta y^+ \propto Pr^{-1/3}$.

343 Pr has implications for the overall temperature profile across the channel gap in stratified
 344 plane Couette flows, as we discuss in detail in §4.

345 3.3. Damping functions

346 To complete the mixing length specifications by taking into account the near-wall
 347 layer and the effect of Pr mentioned above, one can apply the van Driest damping
 348 functions (van Driest 1956) to the mixing lengths in (3.13). This near-wall correction
 349 improves the modelling of the turbulent fluxes in terms of their dependence on y_w in the
 350 viscous/conductive sublayer (Pope 2000). The momentum mixing length is corrected by
 351 the damping function $D_m(y^+)$ to become

$$\ell_m^* = k_m y_w \Phi_m^{-1}(\xi) D_m(y^+) = k_m y_w \Phi_m^{-1}(\xi) [1 - \exp(-y^+/A_m^+)], \quad (3.22)$$

352 where the van Driest constant for momentum A_m^+ is set to be 26 (van Driest 1956; Pope
 353 2000).

354 Similarly, the scalar mixing length becomes

$$\ell_s^* = k_s y_w \Phi_s^{-1}(\xi) D_s(y^+) = k_s y_w \Phi_s^{-1}(\xi) [1 - \exp(-Pr^{-1}y^+/A_s^+)], \quad (3.23)$$

355 where the constant A_s^+ is inherently related to the Pr -dependent additive constant C_s
 356 in (3.16) (Pope 2000) and is thus also a function of Pr .

357 As $y^+ \rightarrow 0$, the turbulent diffusivity κ_t in the conductive sublayer, following (3.23),
 358 scales as

$$\kappa_t = \ell_s^* u^* = \ell_s^* \ell_m^* \left| \frac{dU}{dy} \right| \sim k_s k_m \frac{y^{+4}}{A_s^+ A_m^+} \frac{\nu}{Pr} \sim k_s k_m \frac{y^{+4}}{A_s^+ A_m^+} \kappa. \quad (3.24)$$

359 Note that (3.24) does not yield the expected power law, i.e. $\kappa_t \propto y^3$, that describes the
 360 near-wall variation of κ_t , which is a shortcoming of the van Driest model (see Pope (2000),
 361 pg 305). We use the standard van Driest model for its simplicity. More sophisticated near-
 362 wall treatments for large Prandtl (Schmidt) number can be found in e.g. van Reeuwijk

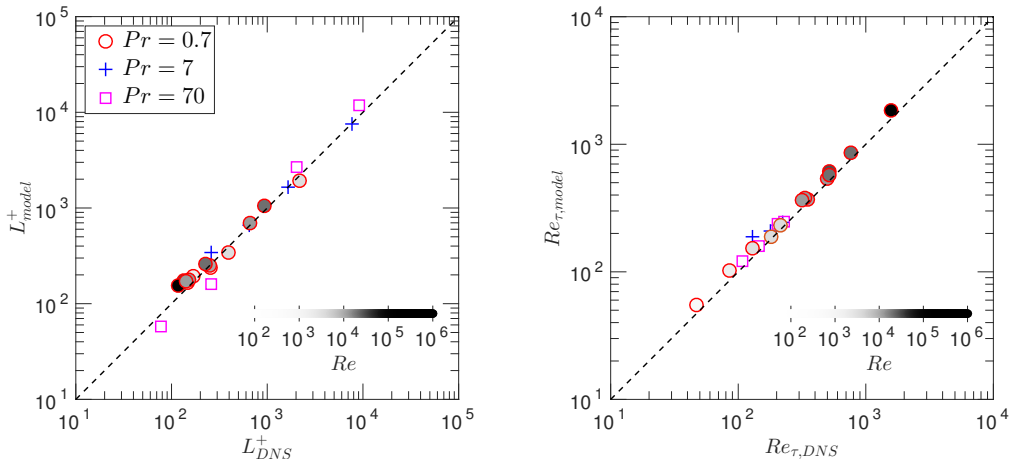


Figure 4: Comparison of the model prediction of L^+ and Re_{τ} with DNS data from the present study and Deusebio *et al.* (2015). L^+_{model} and $Re_{\tau,\text{model}}$ are the results of the mixing length model as described in §3; L^+_{DNS} and $Re_{\tau,\text{DNS}}$ are the results of DNS which are tabulated in Table 1. Varying Reynolds numbers are used in the simulations with $Pr = 0.7$ (plotted with circles) and the fill colour is made darker for larger values of Re .

363 & Hadziabdić (2015). The inclusion of Pr^{-1} in the scalar damping function $D_s(y^+)$ in
 364 (3.23) is such that κ_t in the near-wall limit is proportional to the molecular diffusivity κ
 365 (rather than $\nu = \kappa Pr$).

366 The quantity A_s^+ is, by definition, a dimensionless wall distance below which the
 367 damping takes place. A natural choice for A_s^+ is to take $A_s^+ \sim \Delta y^+$ where the latter
 368 is a characteristic height of the conductive sublayer as defined by (3.19). In this model,
 369 we take $A_s^+ = 0.65\Delta y^+$. This results in A_s^+ values of $\{7.9, 4.3, 2.1\}$ respectively for
 370 $Pr \in \{0.7, 7, 70\}$.

371

3.4. Comparisons with DNS

372

373 This Monin–Obukhov mixing length model as described above can be implemented to
 374 produce predictions of wall fluxes u_{τ}^2 and q_w and the dimensionless parameters defined
 375 in terms of the various fluxes, given the external parameters Re , Ri and Pr . Figure 4
 376 shows the comparisons between the model predictions of $L^+ \equiv L/\delta_{\nu}$ and $Re_{\tau} \equiv h/\delta_{\nu}$
 377 (see definitions in (1.3) & (2.6) respectively) and DNS results at $Re = 4250$ (the present
 378 study) and a (crucially) wider range of Re values (Deusebio *et al.* 2015) as listed in table
 379 1. Given the considerable range of parameters, the agreement of the model predictions
 380 with DNS data is reasonable, with the L_2 norm of percentage relative errors being 16.4%
 381 for L^+ and 13.9% for Re_{τ} over all simulations tested in figure 4. We believe that the
 382 model is thus validated and can be employed to produce an estimate of the wall fluxes
 given the (externally set) (Re, Ri, Pr) parameters.

383 4. Effects of Prandtl number

384

385 In this section, we examine the DNS results focusing on the effects of the Prandtl
 386 number Pr , which is the first main theme of this paper. In particular, we will address the
 387 three main questions already posed in the Introduction: i) how does Pr modify the mean
 flow/temperature profiles; ii) what do these modifications imply for the momentum and

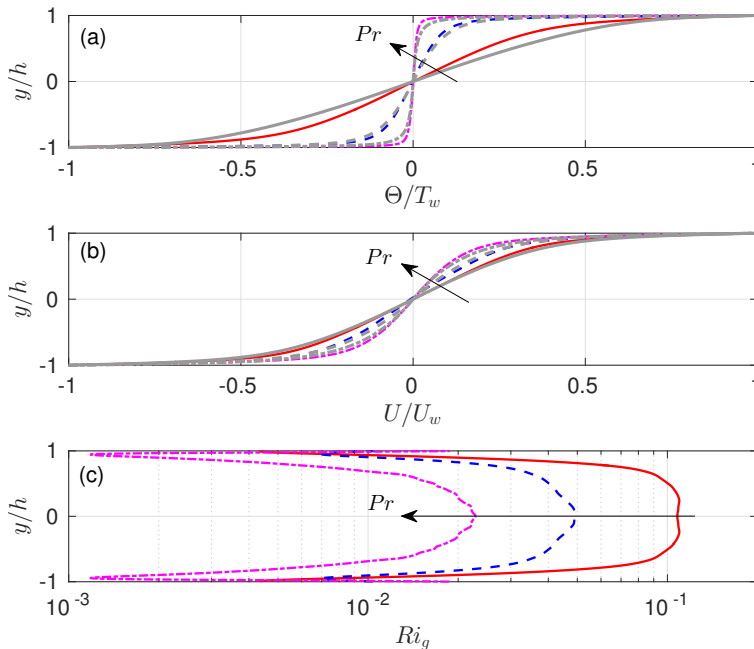


Figure 5: Vertical profiles of: (a) mean temperature Θ/T_w ; (b) mean velocity U/U_w ; and (c) gradient Richardson number Ri_g at $(Re, Ri) = (4250, 0.04)$. The results of simulation 3 with $Pr = 0.7$ are plotted with a solid line; the results of simulation 6 with $Pr = 7$ are plotted with a dashed line; and the results of simulation 9 with $Pr = 70$ are plotted with a dot-dashed line. For reference, in panels *a* & *b*, grey lines with the corresponding line type for each Pr show the predictions of the mixing length model described in §3.

388 heat fluxes through the wall; and iii) how does the intermittency boundary, delineated
 389 in the (Re, Ri) space, vary with Pr ?

390 Figure 5 shows the effects of Pr on the mean velocity (U) and mean temperature (Θ)
 391 profiles in the wall-normal y -direction. At fixed values of $(Re, Ri) = (4250, 0.04)$, the
 392 mean temperature gradient $d\Theta/dy$ (plotted in figure 5(a)) sharpens significantly in the
 393 near-wall region, as Pr increases by two orders of magnitudes from 0.7 to 70. On the
 394 other hand, the vertical variation of Θ weakens in the interior of the channel gap away
 395 from the walls with increasing values of Pr . The gradient Richardson number (plotted
 396 in figure 5(c)), is defined as

$$Ri_g(y) \equiv \frac{N^2}{S^2} = \frac{-(g/\rho_0)(d\bar{\rho}/dy)}{(dU/dy)^2} = \frac{g\alpha_V(d\Theta/dy)}{(dU/dy)^2}, \quad (4.1)$$

397 where $S \equiv dU/dy$ denotes the mean vertical shear and U is the mean velocity as defined
 398 in (2.3). Ri_g varies sharply in the near-wall region and reaches a plateau in the channel
 399 gap interior. Given that the mean shear S (plotted in figure 5(b)) is less sensitive to Pr ,
 400 the Ri_g values at mid-gap ($y = 0$) decrease with Pr at fixed values of (Re, Ri) , which
 401 is mainly attributed to the sharpening of $d\Theta/dy$ in the near-wall region and weakening
 402 of those gradients (and thus the strength of stratification, as measured by N^2) in the
 403 channel gap interior.

404 We now examine the effects of Pr on Nu , Re_τ and L^+ , dimensionless quantities which
 405 are determined by the wall fluxes of heat and momentum. As shown by DCT, critical to

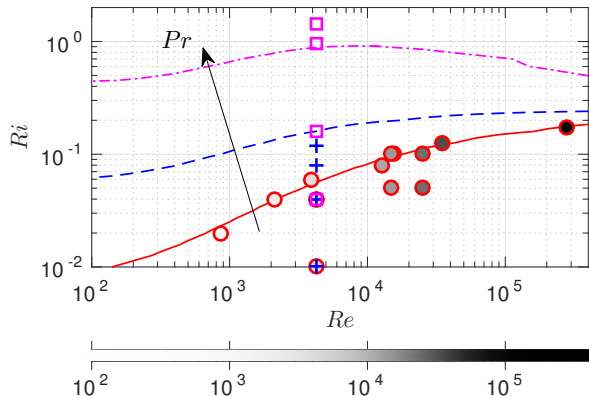


Figure 6: Effect of Pr on the intermittency boundary on the (Re, Ri) plane. Contours corresponding to $L^+ = 200$, the minimum L^+ value for fully developed turbulence (no intermittency) as proposed by DCT, are constructed using the mixing length model described in §3. The areas corresponding to $L^+ > 200$ are *below* the various contour line, plotted with a solid line for $Pr = 0.7$, with a dashed line for $Pr = 7$ and with a dot-dashed line for $Pr = 70$. The (Re, Ri) combinations for the simulations (see table 1) considered in the present study are marked with circles for $Pr = 0.7$, with pluses for $Pr = 7$ and with squares for $Pr = 70$. Varying Reynolds numbers are used in the simulations at $Pr = 0.7$, and the fill colour in the circles is made darker for larger values of Re to match figure 4.

406 the transition from intermittent behaviour to fully turbulent behaviour is the parameter
 407 L^+ , which can be rewritten in terms of the bulk input external parameters (Re, Ri, Pr)
 408 and the output parameters (Re_τ, Nu) as

$$L^+ = \left(\frac{1}{k_m Re^2 Ri} \right) \left(\frac{Re_\tau^4}{Nu/Pr} \right). \quad (4.2)$$

409 Consider the scenario where (Re, Ri) are fixed and Pr is adjusted by varying κ . The first
 410 bracket on the right hand side of (4.2) is thus fixed, and the second bracket includes
 411 all parameters that are Pr -dependent. The term Re_τ^4 is a measure of momentum flux
 412 (shear stress), and the term $Nu/Pr = q_w h / (T_w \nu)$ quantifies the stabilizing effect of
 413 stratification. By inspecting the values of Re_τ and Nu in table 1 as they vary with Pr ,
 414 (in particular, simulations 3, 6 and 9 which share the same (Re, Ri)) it appears that
 415 Re_τ increases and Nu/Pr decreases as Pr increases. In combination, these two effects
 416 result in larger values of L^+ . Therefore, at given (Re, Ri) values, larger Pr enhances
 417 the destabilizing wall shear stress and inhibits the stabilizing heat flux. The flow thus
 418 becomes more prone to turbulence due to the increase of Pr .

419 Figure 6 demonstrates the effect of Pr on the intermittency boundary dividing the fully
 420 turbulent flow regime from the intermittent regime. Contours corresponding to $L^+ = 200$,
 421 i.e. the intermittency boundary proposed by DCT, are plotted on the (Re, Ri) plane. At
 422 a given Re , increasing Pr effectively allows fully turbulent flows to exist at higher values
 423 of Ri . This can be understood from two perspectives. First, as discussed previously,
 424 increasing Pr destabilizes the flow due to the combined effects of larger shear and smaller
 425 stratification. Second, Pr reshapes the mean temperature and velocity profiles which
 426 results in smaller gradient Richardson number Ri_g values in the channel gap interior as

427 Pr increases (as shown in figure 5) allowing shear to dominate stratification away from
 428 the walls. While large values of Pr can raise the transitional Ri value for a given Re ,
 429 figure 6 suggests that fully developed turbulence is not likely to exist for $Ri \gg 1$, at
 430 least within the range of Re and Pr values which has been investigated, both for the
 431 simulations conducted specifically for this paper at $Re = 4250$, and the simulations at a
 432 range of Re presented by DCT, as listed in table 1.

433 5. Monin–Obukhov similarity scaling

434 It has been shown in §4 that Pr plays a significant role in the *near-wall* region by
 435 modulating the wall heat flux q_w , the momentum flux u_τ^2 and thus the dimensionless
 436 parameters such as L^+ and Re_τ . In this section, we turn our attention to our second
 437 main theme, i.e. assessing the validity of Monin–Obukhov similarity scaling. We focus
 438 on the turbulence in the *interior* of the channel gap and examine how the turbulence
 439 characteristics relate to the wall fluxes q_w and u_τ^2 . Scalings for various flow diagnostics
 440 are formulated in the context of Monin–Obukhov theory (see details in appendices
 441 A and B, and the similar formulations considered independently by Scotti & White
 442 (2016)). These predictions are then compared to DNS data shown in figure 7 and the
 443 dynamical implications of these scalings are discussed in detail in this section. Simulations
 444 specifically performed for the present study, i.e. simulations 1–12 as listed in table 1, which
 445 cover a wide range of Pr , as well as those performed by DCT, i.e. simulations 13–23,
 446 which cover a wide range of Re , are included in our discussions.

447 5.1. Equilibrium Richardson number

448 We first revisit the mid-gap gradient Richardson number $Ri_g|_{y=0}$ for fully developed
 449 stationary (equilibrium) stratified plane Couette flows as prescribed by Monin–Obukhov
 450 scaling. The concept of just such a characteristic equilibrium Ri_g value was discussed
 451 by Turner (1973) in the context of constant flux layers. There also exists a large body
 452 of literature considering the ‘stationary Richardson number’ in homogeneous sheared
 453 stratified turbulence, e.g. see Shih *et al.* (2000), where the particular value of the gradient
 454 Richardson number is imposed by construction, and the references therein. A more recent
 455 discussion by Galperin *et al.* (2007) questioned whether such a unique ‘critical Richardson
 456 number’ exists, although the flows considered there differed in several significant ways
 457 from the flows considered here. Specifically, and most importantly, stratified plane
 458 Couette flow exhibits intermittency for the bulk Richardson number $Ri \lesssim O(1)$. Also,
 459 as we discuss in more detail below, the turbulent Prandtl number, i.e. the ratio of
 460 eddy diffusivities of heat and momentum, behaves in a qualitatively different manner in
 461 stratified plane Couette flow from the behaviour of the ‘quasi-normal scale elimination’
 462 (QNSE) model used in Galperin *et al.* (2007). Under the plausible assumption that
 463 a critical Richardson number exists at least in the flow geometry under consideration
 464 here, it may help us to assess if the turbulence would be self-sustained if the externally
 465 imposed Richardson number matches the equilibrium condition, or if the flow would self-
 466 adjust under the non-equilibrium conditions (Turner 1973). Examples of the adjustment
 467 in the latter scenario include the formation of ‘layer’ and ‘interface’ structures through
 468 the rearrangement of velocity and density profiles so that the equilibrium Richardson
 469 number is maintained everywhere in the vertical direction (see §10, Turner (1973)).

470 Figure 7(a) compares the mid-gap equilibrium $Ri_g|_{y=0}$ values from DNS data (from
 471 both the present study and those by DCT crucially at a range of Re) with the model

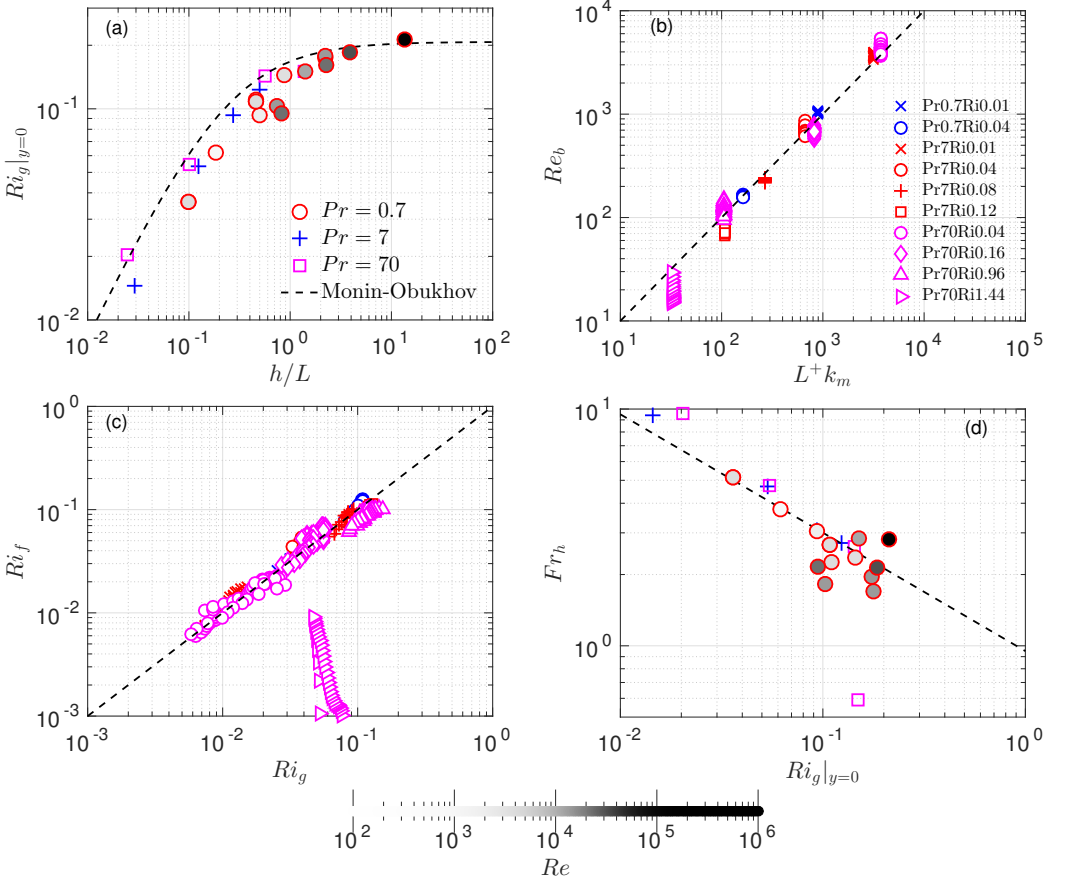


Figure 7: DNS verification of the Monin–Obukhov scalings (5.1), (5.3), (5.4) and (5.7). (a) Equilibrium gradient Richardson number $Ri_g|_{y=0}$ at mid-gap, as a function of length scale ratio h/L . (b) Buoyancy Reynolds number Re_b as a function of length scale ratio L^+ . Re_b values are computed pointwise in y for the channel gap interior with $y^+ > 50$. (c) Flux Richardson number $Ri_f \equiv -B/P$ as a function of gradient Richardson number Ri_g . Ri_f and Ri_g values are computed pointwise in y in the channel gap interior with $y^+ > 50$. Symbol types are the same as panel b. (d) Turbulent Froude number Fr_h as a function of mid-gap gradient Richardson number Ri_g . Fr_h is estimated as $\varepsilon/(Nu_\tau^2)$, where ε and N are sampled at mid-gap $y = 0$. Symbol types are the same as in panel a. The dashed line corresponds to $Fr_h = 0.95 Ri_g^{-1/2}$, the least-squares fit to the scaling (5.7). In panels a & d, the fill colours of the circles (corresponding to simulations with $Pr = 0.7$) are made darker for larger values of Re .

472 prediction (B3) derived in appendix B, i.e.

$$Ri_g|_{y=0} = \frac{k_m}{k_s} \frac{(h/L)^{-1} + \beta_s}{[(h/L)^{-1} + \beta_m]^2}, \quad (5.1)$$

473 which suggests that such an equilibrium Ri_g value is determined solely by the length
 474 scale ratio h/L (note that k_m , k_s , β_s and β_m are model constants defined in §3). The
 475 data points indeed collapse in figure 7(a) for the wide range of external parameters (in

particular, Prandtl number Pr , but also Reynolds number Re) examined, and the DNS results compare well with the Monin–Obukhov prediction (5.1).

Two scenarios in stratified plane Couette flows arise from (5.1) when h/L approaches different limits. First, when $h/L \rightarrow \infty$, the mid-gap equilibrium Ri_g saturates at

$$Ri_g|_{y=0} = \frac{k_m \beta_s}{k_s \beta_m^2} \simeq 0.21. \quad (5.2)$$

This scenario is at least superficially similar to the discussion of constant-flux layers in ‘very stable’ stratification (Ellison 1957; Turner 1973), although as discussed further below, the behaviour of the turbulent Prandtl number is qualitatively different from that assumed by Ellison (1957). When $\xi = h/L \gg 1$, the *linear* dependence of Monin–Obukhov functions Φ_m and Φ_s on ξ dominates (see (3.11) and (3.12)). Fluid in the channel gap interior does not ‘feel’ the impact of the wall directly (but still indirectly through the wall fluxes u_w^2 and q_w), because the vertical motions are strongly damped by stratification. In the channel gap interior, the distance to the wall y_w (or the channel gap half-height h) becomes irrelevant, as shear and temperature gradients both become constant (by taking the limit of (3.12) at $\xi \rightarrow \infty$), which renders the turbulence close to homogeneous in the wall-normal direction. Interestingly, the *maximum* stationary Ri_g reported in homogeneous sheared turbulence is also approximately 0.2 (see e.g. Shih *et al.* (2000)). This reinforces the notion that Monin–Obukhov scaling may also apply to such homogeneous triply-periodic flows (Chung & Matheou 2012). There remains some debate as to whether the standard Monin–Obukhov theory holds in the $\xi \rightarrow \infty$ limit in a stable atmospheric boundary layer, see for example the discussion on ‘ z -less’ stratification by Mahrt (1999), and any such differences between the standard theory and boundary layer flow are likely linked to the variation of fluxes with height in a real boundary layer. However, the statistically stationary stratified plane Couette flows examined here, which are constant-flux layers by construction, appear to be consistent with the standard Monin–Obukhov theory.

As an aside, we note that this maximum observed Richardson number is close to $Ri_g = 1/4$ which arises in the well-known Miles–Howard criterion for linear normal mode stability of inviscid parallel steady stratified shear flows (Miles 1961; Howard 1961). This closeness is apparently fortuitous, as the arguments leading to the prediction of the value in (5.2) are entirely constructed under the assumption of statistically stationary turbulent flow. Therefore, it is at least possible that observations of Ri_g close to $1/4$, as, for example, in the Equatorial Undercurrent (Smyth & Moum 2013), are due to turbulent balances, not ‘marginal stability’ of the flow, as argued by Thorpe & Liu (2009), although, it is also important to remember, as shown for example by Pham *et al.* (2013), that the dynamics of the Equatorial Undercurrent is inevitably non-stationary, due to diurnal forcing.

Second, when h/L is $O(1)$ or smaller, the equilibrium Ri_g at mid-gap varies strongly with h/L , which can be seen from figure 7(a). Under this scenario, the stabilising effects due to stratification are relatively weak. The direct influence of the walls on the interior turbulence becomes significant, and both h and L become relevant scales for the channel gap interior.

5.2. L^+ , Re_b and intermittency

The parameter L^+ is a useful diagnostic quantity to predict if stratified plane Couette flows can sustain a fully turbulent state or become intermittent (as discussed by DCT). On the other hand, the buoyancy Reynolds number $Re_b \equiv \varepsilon/(\nu N^2) \sim (\ell_O/\eta)^{4/3}$, which describes the scale separation between the Ozmidov scale ℓ_O and the Kolmogorov scale η , is often used to predict whether small scale turbulence can exist given the level of

522 turbulent dissipation and stratification (see e.g. Riley & Lindborg (2012)), typically in
 523 homogeneous simulations (Brethouwer *et al.* 2007).

524 A natural question to ask is then whether L^+ and Re_b are related to each other, at
 525 least in stratified plane Couette flows. The analysis in Appendix B has, through Monin–
 526 Obukhov similarity theory, predicted a linear scaling between L^+ and Re_b as given by
 527 (B5) shown in Appendix B, i.e.

$$Re_b \sim L^+ k_m. \quad (5.3)$$

528 In figure 7(b) this scaling is confirmed from DNS data (shown for simulations 1–12), and
 529 has already been noted by Scotti & White (2016) in a more limited range of $Ri \leq 0.1$,
 530 $Re \leq 55000$ and $Pr = 1$. Re_b estimates presented here are based on ε and N values
 531 that are sampled pointwise in the vertical direction y . However, in open flows, there are
 532 different possible choices of averaging volumes for ε and N (see e.g. Salehipour *et al.*
 533 (2016)), and caution needs to be exercised when comparing specific numerical values of
 534 Re_b between different flow geometries, or indeed between different analyses. A reanalysis
 535 of DCT’s data (simulations 13–23, not shown) suggests the same linear scaling for a wide
 536 range of Re and Ri . This indicates that the L^+ criterion for predicting intermittency,
 537 which is specific to wall-bounded flows, is also linked to this more general Re_b argument.
 538 The critical (minimum) Re_b for fully developed turbulence, as inferred from the $L^+ > 200$
 539 criterion reported by DCT and the scaling (5.3), is approximately 80 (as $k_m \approx 0.4$) for
 540 stratified plane Couette flows. This critical Re_b of 80 is close to the cut-off value $Re_b = 100$
 541 between the ‘intermediate’ and ‘energetic’ regimes of Shih *et al.* (2005) which is discussed
 542 in detail in §6, although one needs to be careful about whether the Re_b value is a ‘bulk’
 543 or local estimate when comparing the numerical values. Here simulation 12 is in the
 544 intermediate regime ($Re_b < 35$, see figure 7(b)), and in what follows, we focus instead
 545 on the other simulations ($Re_b > 60$) which are close to or within this ‘energetic’ regime
 546 in terms of the Re_b value.

547 5.3. Turbulent Prandtl number

548 In appendix B, it is shown through scaling arguments that the flux Richardson number
 549 Ri_f is proportional to Ri_g . The particular scaling derived in Appendix B is given by (B7)
 550 i.e.

$$Ri_f \sim Ri_g, \quad (5.4)$$

551 and is compared to DNS results (simulations 1–12) in figure 7(c). In general, Ri_f is
 552 proportional to Ri_g with a multiplicative constant of approximately unity, which is
 553 consistent with DCT. The group of points which appear to be outliers, correspond to
 554 simulation 12 ($Pr = 70, Ri = 1.44$). As discussed previously, the atypical behaviour
 555 associated with this simulation is likely to be due to low- Re_b , and hence inherently
 556 viscously dominated effects.

557 With the turbulent viscosity ν_t defined through the flux-gradient relation

$$\nu_t \equiv -\frac{\langle u'v' \rangle}{S}, \quad (5.5)$$

558 and turbulent diffusivity κ_t defined in (A5), the turbulent Prandtl number $Pr_t \equiv \nu_t/\kappa_t$
 559 can be expressed as

$$Pr_t = \frac{Ri_g}{Ri_f}. \quad (5.6)$$

560 The $Ri_f \simeq Ri_g$ scaling can thus be interpreted alternatively as the turbulent Prandtl
 561 number Pr_t being approximately unity, which is consistent with the Reynolds analogy,

as noted independently by Scotti & White (2016). This result can be derived from Monin–Obukhov theory (appendix B) and is consistent with DNS data for the present study (simulations 1–12) shown in figure 7(c), as well as from revisited DCT datasets (simulations 13–23) which exhibit the same behaviour (not shown).

Pr_t is often parameterized as a function of Ri_g in the literature (see, for example, Venayagamoorthy & Stretch (2010)). Pr_t being unity, as we observe in stratified plane Couette flows (see figure 7(c)), appears to be typical for gradient Richardson numbers $Ri_g < 0.2$ which are sufficiently small in this context – again, one needs to be careful about the exact definition of Ri_g when comparing across different studies, and also it is necessary to remember that this is distinct from keeping the bulk Richardson number Ri (set by the boundary conditions) small. This observation is consistent with previous studies of stably stratified wall-bounded flow simulations (Armenio & Sarkar 2002; García-Villalba & del Álamo 2011; García-Villalba *et al.* 2011*a*) and in homogeneous stratified turbulence (Rohr & Van Atta 1987; Chung & Matheou 2012).

The behaviour of Pr_t becomes more complex at higher values of Ri_g , i.e. for $Ri_g > 0.2$ (Taylor *et al.* 2005; Venayagamoorthy & Stretch 2010; Karimpour & Venayagamoorthy 2014, 2015; Salehipour & Peltier 2015; Wilson & Venayagamoorthy 2015). However, turbulent flows with larger gradient Richardson numbers $Ri_g > 0.2$ do not appear to be accessible in stratified plane Couette flows, for reasons that have been discussed in §5.1. There also exist Re_b -based parameterizations for Pr_t in the literature. Shih *et al.* (2005) and Salehipour & Peltier (2015) reported Pr_t approaching order unity for intermediate to large values of Re_b , which is consistent with our observations. Salehipour & Peltier (2015) also observed larger than $O(1)$ values of Pr_t when the values of Re_b are small, i.e. $O(1)$ to $O(10)$. This is consistent with our outlier group (simulation 12) in figure 7(c) whose Re_b value is $O(10)$ (see figure 7(b)) and the Pr_t value is larger than unity ($Ri_g \gg Ri_f$).

Crucially, all the evidence points towards $Pr_t \sim O(1)$ while the flow is turbulent, with the flow becoming intermittent before Ri_g reaching large values. This is qualitatively different behaviour to that assumed by Ellison (1957), who stated that ‘it seems more likely’ that turbulence could be ‘maintained’ at large values of Ri_g with still finite $Ri_f < 1$, and so, from (5.6) and consequences derived from it with further turbulence modelling assumptions, Ellison (1957) was led to the conclusion that Pr_t inevitably reaches large values. Galperin *et al.* (2007) analogously arrived at the conclusion that Pr_t reaches large values in strongly stratified, yet still ‘turbulent’ flows, in the relatively weak sense that the eddy diffusivities (particularly in the horizontal) remain elevated above molecular values. A potential major point of difference is the central role played in open flows of propagating internal waves, which is not possible in stratified plane Couette flow.

5.4. Realizability of strongly stratified regime

Finally, we test the scaling in (B 11) in appendix B, i.e.

$$Fr_h \sim \frac{1}{\sqrt{Ri_g}}, \quad (5.7)$$

for the turbulent Froude number Fr_h . Figure 7(d) shows the DNS results for which an empirical scaling of

$$Fr_h \simeq \frac{0.95}{\sqrt{Ri_g}} \quad (5.8)$$

applies, which is consistent with the Monin–Obukhov prediction in appendix B. The outlier once again corresponds to simulation 12 for which the Re_b value may not be high

605 enough for the inertially-dominated forward cascade assumption underlying (B 8), i.e.
 606 $\varepsilon = U'^3/\ell_h$, to hold.

607 Given that the maximum Ri_g in fully developed stratified plane Couette flow is
 608 approximately 0.2 (see §5.1), the minimum Fr_h that can be obtained in the interior
 609 of an stratified plane Couette flow (at large enough Re_b) is approximately 2, following
 610 (5.8). However, for the turbulence to reach the strongly stratified regime, it is typically
 611 argued that Fr_h needs to be smaller than 0.02 (Brethouwer *et al.* 2007). Therefore,
 612 the strongly stratified regime, which is characterised by layering in the density field
 613 with characteristic vertical length scale U'/N , may be fundamentally *nonrealizable* in
 614 stratified plane Couette flows, at least under the equilibrium conditions we have been
 615 considering. Once again, it is important to emphasise that it is the mid-gap gradient
 616 Richardson number Ri_g which cannot become large in quasi-steady turbulent stratified
 617 plane Couette flow, for any choice of Re and Ri set by the boundary conditions.

5.5. Summary

618
 619 To summarize the results in §5, we have identified certain generic characteristics of
 620 the turbulence in the interior regions of stratified plane Couette flows. We find that: the
 621 length scale ratio h/L determines the mid-gap Ri_g ; Re_b scales linearly with $L^+ \equiv L/\delta_\nu$;
 622 Pr_t is of order unity for the range of accessible Ri_g associated with turbulence; and Fr_h
 623 is proportional to $Ri_g^{-1/2}$. The scalings, consistent with, and extending the observations
 624 of Scotti & White (2016) into the crucially important regime where the externally set
 625 bulk $Ri > 0.1$, apply not only to the DNS performed for the present study which cover
 626 a wide range of Pr (simulations 1–12), but also to those by DCT as listed in table 1
 627 which covered a wider range of Re (simulations 13–23). These characteristics of stratified
 628 plane Couette flows fundamentally relate to the fact that it is the upper and lower walls
 629 which impose momentum and heat fluxes on the fluids. These fluxes then dictate the self-
 630 similar behaviour of both the mean flow (as characterised by Ri_g) and the turbulence (as
 631 characterised by Re_b , Pr_t and Fr_h) in the interior. These results are expected to hold not
 632 only for stratified plane Couette flows but also for other constant-flux layers to which the
 633 Monin–Obukhov scaling applies. These Monin–Obukhov scalings are intended for regions
 634 sufficiently far from the walls. Through the wide range of Prandtl numbers examined,
 635 our DNS data suggest that the dynamics away from the walls are Pr -independent for
 636 given wall fluxes.

6. Mixing and its parameterization

6.1. Osborn formulation for stratified plane Couette flow

637
 638
 639 Now we turn our attention to the third main theme of interest, namely the parameter-
 640 ization of mixing. Here we use the framework proposed by Osborn (1980) to formulate
 641 a parameterization for the turbulent diffusivity $\kappa_t \equiv -\langle \rho'v' \rangle / (d\bar{\rho}/dy) = -B/N^2$. As
 642 described in appendix C, key to this formulation is the turbulent flux coefficient, $\Gamma \equiv$
 643 $B/\varepsilon \approx Ri_f/(1 - Ri_f)$. With Γ appropriately parameterized, the Osborn formulation
 644 yields an expression for κ_t , i.e.

$$\frac{\kappa_t}{\nu} \approx \frac{Ri_f}{1 - Ri_f} \frac{\varepsilon}{\nu N^2} = \Gamma Re_b. \quad (6.1)$$

645 It is important to appreciate that key aspects of the Osborn (1980) framework are based
 646 on the theoretical considerations of Ellison (1957) and the experimental data of Britter
 647 (1974), both associated with stratified flows in the presence of boundary forcing and

thus expected to have at least some similar properties to the turbulence in stratified plane Couette flows. Osborn (1980), following Ellison (1957), postulated that $\Gamma \leq 0.2$, or equivalently $Ri_f \leq 0.15$, although the inequality in Osborn’s original paper has often been ignored subsequently. Interestingly, the experimental data by Britter (1974) (see e.g. pg 8-37 of the thesis) led to his conclusion that ‘a critical Richardson flux number (i.e. Ri_f) of approximately 0.2 is predicted’. This is entirely consistent with our results presented in §5 that

$$Ri_f \simeq Ri_g \lesssim 0.2 \quad (6.2)$$

in stratified plane Couette flows for turbulence to be maintained, although as already noted we observe the turbulent Prandtl number remaining of order one, unlike in the model developed by Ellison (1957). Indeed, using this scaling, Γ can be written as a function of the gradient Richardson number Ri_g :

$$\Gamma \approx \frac{Ri_g}{1 - Ri_g}, \quad (6.3)$$

remembering that Ri_g appears to have an upper bound above which turbulence cannot be maintained, even for asymptotically large Re (see figure 18 of DCT). In the literature, however, Γ is often parameterized as a function of Re_b (see e.g. Shih *et al.* (2005)). The connection between the Ri_g -based and Re_b -based scalings for Γ is discussed further in §6.3.1. It follows from (6.1) and (6.3) that

$$\frac{\kappa_t}{\nu} \approx \frac{Ri_g}{1 - Ri_g} Re_b \quad (6.4)$$

in the context of stratified plane Couette flows. Noting that $Pr_t \equiv \nu_t/\kappa_t \approx 1$ in stratified plane Couette flows (as shown in §5) and as also noted by Scotti & White (2016), we can also approximate the turbulent viscosity ν_t with the same scaling for κ_t in (6.4), i.e.

$$\frac{\nu_t}{\nu} \approx \frac{Ri_g}{1 - Ri_g} Re_b. \quad (6.5)$$

6.2. Numerical results

These κ_t and ν_t values are estimated directly using their definitions through the flux-gradient relation (A 5) and (5.5) at all locations in the wall-normal direction y that are at least 50 wall units ($y^+ > 50$) away from the walls, where the local equilibrium (A 3) is expected to hold (García-Villalba *et al.* 2011*b*). These results are first plotted in figure 8 to test the Re_b -based parameterizations that are commonly seen in the literature, e.g. those reviewed by Ivey *et al.* (2008) and also discussed in Scotti & White (2016). Our results are plotted in figure 9 to validate the scalings (6.4) and (6.5). Simulation 12, in which the flow is viscously controlled and exhibits spuriously small ($O(1)$ or smaller) or negative (counter-gradient) values of κ_t/ν or ν_t/ν , is not included in the plots to allow the discussion to stay focused on the fully turbulent simulations.

Figure 8 compares the DNS results of κ_t/ν against the classical Re_b -based parameterizations of Osborn (1980) and Shih *et al.* (2005). The DNS data points in figure 8 are sampled *locally* (pointwise) at various y locations across the channel gap interior of stratified plane Couette flows. Within each simulation, the Re_b value stays relatively constant, while the diffusivities span a wider range – the latter is somewhat expected because κ_t and ν_t scale linearly with the mixing lengths ℓ_s^* and ℓ_m^* respectively, both of which increase with the wall distance y_w , as described in §3.1. These Re_b -based scalings are effective in describing the *homogeneous* flow dataset of Shih *et al.* (2005), but they do not provide a good agreement with our DNS data from stratified plane Couette flows

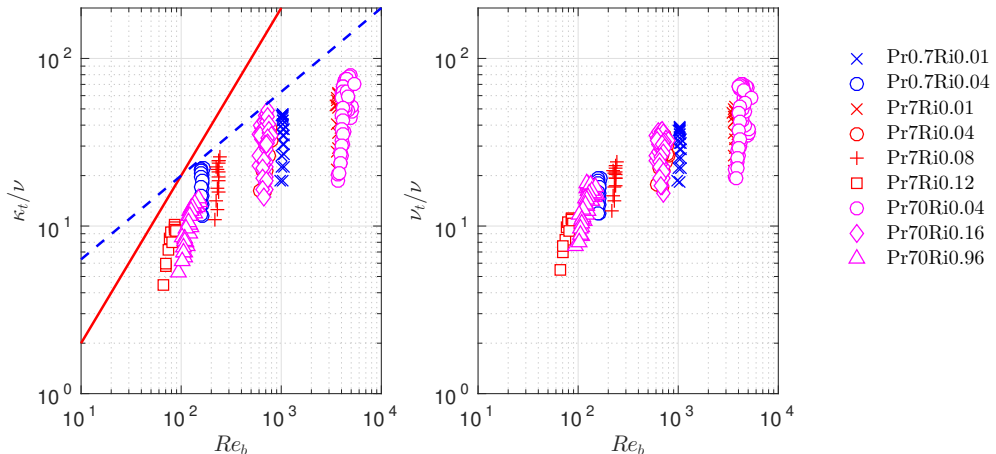


Figure 8: κ_t and ν_t , as defined by (A 5) and (5.5), and both normalised by ν , as a function of Re_b . κ_t , ν_t and Re_b values are computed pointwise in y in the channel gap interior with $y^+ > 50$. Scaling laws of $\kappa_t/\nu = 0.2Re_b$ (Osborn 1980) plotted with a solid line, and $\kappa_t/\nu = 2Re_b^{1/2}$ (Shih *et al.* 2005) plotted with a dashed line, are also shown.

687 which are inherently *inhomogeneous* due in particular to the presence of the wall. The
 688 data for ν_t , which are also plotted in figure 8, behave similarly to κ_t , since the turbulent
 689 Prandtl number $Pr_t \equiv \nu_t/\kappa_t$ is approximately unity (as shown in §5.3).

690 Figure 9 compares the DNS data against the scalings (6.4) and (6.5). The collapse of the
 691 DNS data improves significantly when Ri_g is included in the parameterizations, as they
 692 capture the critical (linear) dependence of Ri_f on Ri_g . At sufficiently large values of Re_b ,
 693 i.e. $Re_b \gtrsim 60$, the $\kappa_t/\nu \sim \nu_t/\nu \sim Re_b Ri_g/(1 - Ri_g)$ scaling, based on the turbulent kinetic
 694 energy budget argument by Osborn (1980) and incorporating Monin–Obukhov scaling for
 695 constant-flux layers to account for the importance of the (coupled) value of Ri_g , provides
 696 an accurate description of the turbulent diffusivity in stratified plane Couette flows. It is
 697 certainly of interest that the Osborn scaling appears to hold, at least qualitatively, even
 698 though the underlying assumption of Ellison (1957) (on which the Osborn scaling is at
 699 least partially based) that Pr_t becomes large is violated in stratified plane Couette flow.
 700 We further discuss this scaling with respect to other previously proposed scalings in the
 701 next subsection.

702 6.3. Discussions

703 6.3.1. Γ vs. Re_b

704 The Shih *et al.* (2005) scalings parameterize the turbulent flux coefficient Γ as a
 705 function of the buoyancy Reynolds number Re_b , whereas in the context of stratified plane
 706 Couette flow, we propose to parameterize Γ as a function of the gradient Richardson
 707 number Ri_g , i.e. $\Gamma \approx Ri_g/(1 - Ri_g)$. Here we discuss our results further with respect to
 708 the two approaches. Following Shih *et al.* (2005), for $7 < Re_b < 100$, i.e. the ‘intermediate’
 709 regime, a constant turbulent flux coefficient of $\Gamma = 0.2$, as originally proposed by Osborn
 710 (1980) as an upper bound, is used. For $Re_b > 100$, i.e. the ‘energetic’ regime, Γ was
 711 observed by Shih *et al.* (2005) to decrease with Re_b as $\Gamma \propto Re_b^{-1/2}$, although their
 712 data only extend to $Re_b \simeq 900$. The scaling for $Re_b > 100$ appears to be consistent with
 713 numerical data of mixing layers (Salehipour & Peltier 2015) and field observations (Davis

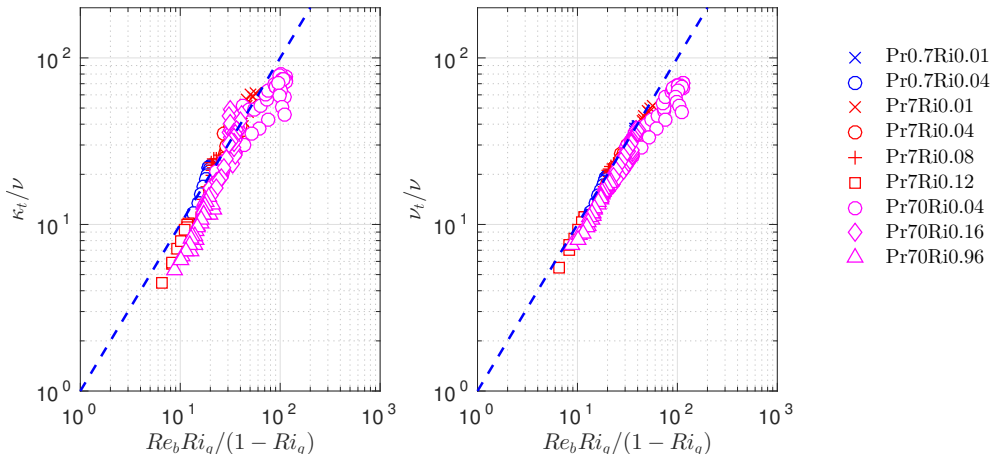


Figure 9: κ_t and ν_t , both normalised by ν , as a function of $Re_b Ri_g / (1 - Ri_g)$. κ_t , ν_t , Re_b and Ri_g values are computed pointwise in y in the channel gap interior with $y^+ > 50$. The dashed line marks equality between the abscissa and the ordinate.

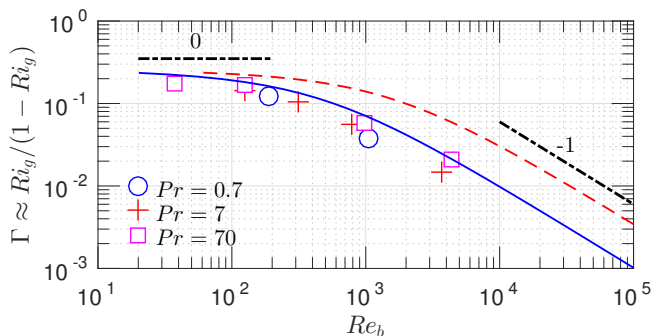


Figure 10: Turbulent flux coefficient Γ (as defined in (C3)) approximated by $Ri_g / (1 - Ri_g)$, where Ri_g is evaluated at mid-gap, plotted as a function of Re_b which is approximated by $k_m L^+$ (as shown in figure 7(b)). Symbols correspond to DNS data. Lines correspond to two different Monin-Obukhov predictions: at $Re = 4250$ (the same Re value as the shown DNS results) plotted with a solid line; and at $Re = 42500$ plotted as a dashed line. Power-law scalings $\Gamma \propto Re_b^n$ with various n values are plotted with dot-dashed lines marked with the values of n .

714 & Monismith 2011; Walter *et al.* 2014). One shortcoming of this scaling is, however, that
 715 the value of $\kappa_t / \nu = \Gamma Re_b \propto Re_b^{1/2}$ becomes infinite when one considers the mixing of
 716 a passive scalar, since $Re_b \rightarrow \infty$ as $N^2 \rightarrow 0$ and ε and ν remain finite. In contrast,
 717 experiments by Holford & Linden (1999) suggested that the eddy diffusivity approaches
 718 a finite value in the zero-stratification limit. Moreover, Chung & Matheou (2012) also
 719 reported saturation of eddy diffusivity for large-to-infinite values of Re_b and offered a
 720 phenomenological explanation from the perspective of competing length scales.

721 The scalings (6.4) and (6.5), by including the Ri_g -dependence, circumvent this problem
 722 at the zero-stratification limit where $Re_b \rightarrow \infty$ as $Ri \rightarrow 0$, as $\Gamma \propto Re_b^{-1}$ in the limit of
 723 $Re_b \rightarrow \infty$ (as shown in figure 10). These scalings also provide a convenient framework to
 724 interpret the change of power-law exponent in Re_b in the scaling of Γ (Barry *et al.*

2001; Shih *et al.* 2005). This is demonstrated in figure 10, where the characteristic
 values of turbulent flux coefficient Γ in the interior of stratified plane Couette flow,
 as approximated by $Ri_g/(1 - Ri_g)$, are plotted against the corresponding Re_b values.
 The Monin–Obukhov predictions from the model presented in §3 are also shown in figure
 10 for two values of bulk Reynolds number Re , i.e. $Re = 4250$ and $Re = 42500$.

As shown in figure 10, when Re_b is smaller than $O(100)$, which corresponds to the
 $h/L > 1$ regime in terms of the characteristic Ri_g value (see figure 7(a)), Ri_g remains
 a constant value of approximately 0.2 at mid-gap as given in (5.2). The characteristic
 turbulent flux coefficient $\Gamma \approx Ri_g/(1 - Ri_g) \approx 0.25$ is thus a constant. This regime
 is reminiscent of Shih *et al.* (2005)’s ‘intermediate’ regime where Γ is a constant of
 0.2 independent of Re_b , the upper bound as argued by Osborn (1980). Consequently,
 $\kappa_t/\nu = \Gamma Re_b \propto Re_b$ in this regime. This regime may be thought of as a saturated regime
 for Γ , as Ri_g is close to its maximum value for sustained turbulence, consistent with the
 underlying assumptions of Osborn (1980).

When Re_b is large, e.g. $Re_b > O(1000)$ for $Re = 4250$, which corresponds to the
 $h/L \ll 1$ limit in terms of Ri_g (figure 7(a)), the characteristic Ri_g can be estimated via
 (B3) by taking the limit of $h/L \rightarrow 0$ or $L^+ \rightarrow \infty$, which yields

$$Ri_g = \frac{k_m h}{k_s L} = \frac{k_m}{k_s} \frac{Re_{\tau,\infty}}{L^+} \approx \frac{k_m^2}{k_s} \frac{Re_{\tau,\infty}}{Re_b}, \quad (6.6)$$

where $Re_{\tau,\infty}$ denotes the friction Reynolds number for the case of passive scalar ($L^+ \rightarrow$
 $\infty, Re_b \rightarrow \infty$). With $Ri_g \ll 1$ in this limit, $\Gamma \approx Ri_g/(1 - Ri_g) \approx Ri_g$. Following (6.6),
 the turbulent flux coefficient $\Gamma \approx Ri_g \propto Re_b^{-1}$ holds for large Re_b in the limit of zero
 Richardson number. It is important to appreciate that this is not in itself inconsistent
 with Osborn (1980)’s argument, as 0.2 is the upper bound he proposes for Γ . It follows
 from (6.6) that, in the limit of $Re_b \rightarrow \infty$, $\kappa_t/\nu = \Gamma Re_b = \frac{k_m^2}{k_s} k_s^{-1} Re_{\tau,\infty}$ approaches a
 constant which depends solely on $Re_{\tau,\infty}$ (which itself is a function of the bulk Reynolds
 number Re). This regime corresponds to the scenario of mixing a nearly passive scalar,
 a regime that finds no counterpart in the regimes presented in Shih *et al.* (2005). As is
 apparent in figure 10, this regime only really becomes clearly identifiable for $Re_b \gtrsim 1000$,
 larger values than those presented in Shih *et al.* (2005).

There exists a transitional regime where Γ decays monotonically with Re_b , but with a
 slower rate than the $\Gamma \propto Re_b^{-1}$ power law in the weakly stratified limit. This transitional
 regime at least superficially resembles Shih *et al.* (2005)’s ‘energetic’ regime where $\Gamma \propto$
 $Re_b^{-1/2}$ and $\kappa_t/\nu \propto Re_b^{1/2}$ in the sense that Γ starts to decrease with Re_b . Of course it is
 important to remember that this resemblance may be entirely fortuitous, due not least to
 the necessity of connecting two different asymptotic regimes, and the marked difference
 of the two flow geometries and forcing mechanisms of the turbulence. The critical Re_b ,
 which marks the transition from the small- Re_b regime to this intermediate- Re_b regime,
 appears to be approximately 100 for $Re = 4250$. However, as shown by Monin–Obukhov
 predictions plotted in figure 10 for $Re = 42500$, the exact value of the critical Re_b is not
 unique but rather moves to larger values for larger Re , and also the specific numerical
 values are dependent on the averaging volumes for ε and N in spatially inhomogeneous
 flows.

To summarize, in the small- Re_b regime with $Re_b \lesssim 100$, Γ and Ri_g are independent
 of Re_b , and in the weakly stratified $Re_b \gtrsim 1000$ regime with small Ri , $\Gamma \approx Ri_g \propto Re_b^{-1}$
 where the mixing resembles that of a nearly passive scalar. It is within the transitional
 regime between these two where Ri_g , and thus also $\Gamma \approx Ri_g/(1 - Ri_g)$, both become
 dependent on Re_b . The coupling between Ri_g and Re_b , as is dictated by Monin–Obukhov

771 scalings in stratified plane Couette flow, may offer some explanation for the commonly
 772 observed variations of Γ with respect to Re_b (as presented, for example, in Shih *et al.*
 773 (2005)). It is very important to stress that this picture emerges from wall-bounded
 774 stratified shear flows, consistent with the arguments and data underpinning the model of
 775 Osborn (1980). In particular, the picture depends strongly on the observation in stratified
 776 plane Couette flow that $Ri_f \simeq Ri_g$ and that $Ri_g \lesssim 0.2$ for sustained turbulence.

777 6.3.2. Γ vs. Fr_h

778 A recent study by Maffioli *et al.* (2016) utilised the parameter Fr_h to scale turbulent
 779 flux coefficient Γ in triply periodic body-forced turbulence. Critically its forcing is very
 780 different from the forcing which we consider. In stratified plane Couette flow, the forcing
 781 at the boundary has to penetrate into the interior to drive turbulent mixing, while the
 782 forcing in the flow considered by Maffioli *et al.* (2016) is introduced throughout the
 783 interior of the flow, and so there is no dynamical ‘barrier’ to the energy being available
 784 to stratified turbulent mixing throughout the flow. For the $Fr_h > 1$ regime, which
 785 corresponds to our small- Ri_g weakly stratified regime, they proposed that $\Gamma \propto Fr_h^{-2}$. A
 786 similar dependence of Γ on the bulk Froude number $Fr_0 = U/\sqrt{G'H \cos \theta}$ (defined using
 787 characteristic scales for the current velocity U along a slope of angle θ to the horizontal,
 788 depth H and reduced gravity $G' \cos \theta$) i.e. $\Gamma \propto Fr_0^{-2}$, has also been reported for relatively
 789 weakly stratified density currents when $Fr_0 \gg 1$ (Wells *et al.* 2010). It has been shown
 790 that $Fr_h \propto Ri_g^{-1/2}$ holds in stratified plane Couette flows (see §5.4), and therefore the
 791 $\Gamma \propto Fr_h^{-2}$ scaling for Γ is consistent with our approximation $\Gamma \approx Ri_g/(1 - Ri_g) \approx Ri_g$
 792 (for small Ri_g). For the small- Fr_h regime, Maffioli *et al.* (2016) reported a Γ value
 793 approaching a constant 0.33 at Fr_h values of $O(10^{-2})$ which are accessible in their forced
 794 simulations. In stratified plane Couette flows, where the minimum Fr_h is of $O(1)$ as
 795 shown in figure 7(d), our results suggest a fixed value of $0.2/(1 - 0.2) = 0.25$ that is
 796 closer to the upper bound of the Osborn (1980) formulation, i.e. $\Gamma = 0.2$, which is also
 797 the value reported by Wells *et al.* (2010) in their intermediate $Fr_0 \sim 1$ regime.

798 6.3.3. *Non-monotonic mixing?*

799 Pioneering work on turbulent mixing in stratified flows (Linden 1979, 1980; Fernando
 800 1991; Park *et al.* 1994; Holford & Linden 1999) revealed the possibility of non-monotonic
 801 behaviour in the stratified mixing, i.e. the buoyancy flux does not necessarily increase
 802 monotonically but rather can plateau and then decrease with increasing stratification.
 803 Non-monotonic mixing was proposed to be the mechanism for the formation of generic
 804 features in stratified fluids such as relatively well-mixed and deep ‘layers’ separated by
 805 relatively shallow and sharp ‘interfaces’, as originally proposed by Phillips (1972). Such
 806 non-monotonic mixing has also been observed in time-dependent stratified shear layers
 807 (Caulfield & Peltier 2000; Smyth *et al.* 2001; Mashayek *et al.* 2013; Salehipour & Peltier
 808 2015). Potentially associated spontaneous layer formation has been observed in stratified
 809 Taylor-Couette flows in the annular region between two concentric cylinders (Ogletorpe
 810 *et al.* 2013) and in flows where the mixing is induced by translating rods (Park *et al.*
 811 1994; Holford & Linden 1999).

812 In fully developed turbulent stratified plane Couette flow, however, such non-monotonic
 813 mixing is not observed. The turbulent flux coefficient $\Gamma \equiv B/\varepsilon$, which measures the
 814 buoyancy flux in dimensionless form, increases monotonically with Ri_g , a dimensionless
 815 measure of the stratification. We hypothesize that this behaviour is due to the range of
 816 Ri_g which is accessible in turbulent stratified plane Couette flows where the maximum
 817 gradient Richardson number is approximately 0.2 (as discussed in §5.1). Effectively, it
 818 appears that stratified plane Couette flows can only access the weakly stratified ‘left flank’

819 of the non-monotonic mixing curve with stratification postulated by Phillips (1972) and
 820 observed widely in experiments (see, for example, the classic review of Linden (1979)).

821 6.3.4. Effect of Prandtl number

822 Throughout our discussion in this section, there is no explicit dependence of the
 823 normalised values of κ_t/ν (or ν_t/ν) on the molecular Prandtl number Pr . This is
 824 probably due to the fact that the Re_b values examined here are sufficiently large, i.e.
 825 $Re_b \gtrsim 60$ (see figure 8), so that the molecular properties of the fluid have no effect on
 826 the turbulent mixing in the channel gap interior. Variation in Prandtl number Pr may
 827 indeed be important for a small- Re_b ‘molecular’ regime with $Re_b \sim O(1 - 10)$ (Shih
 828 *et al.* 2005; Ivey *et al.* 2008; Bouffard & Boegman 2013) which is not the focus of the
 829 present study. Motivated by experimental results, Barry *et al.* (2001) included Pr in their
 830 parameterizations of κ_t even at large values of Re_b up to $O(10^4 - 10^5)$. This discrepancy,
 831 similarly to the situation with respect to Maffioli *et al.* (2016), is most likely associated
 832 with the differences in turbulence forcing mechanisms, i.e. shear driven by the walls as
 833 in the present study, versus grid stirring as in Barry *et al.* (2001) .

834 7. Concluding remarks

835 In this paper, we have investigated stratified turbulence in fully developed stratified
 836 plane Couette flows, through DNS at a wide range of Pr . We use Monin–Obukhov
 837 similarity theory as a guide to interpret the numerical results. In particular, we have
 838 highlighted the relevance of heat and momentum fluxes to the turbulence characteristics
 839 in the channel gap interior, as well as the implications of these similarity scalings for
 840 diapycnal mixing.

841 The dynamical role of Prandtl number appears to be subtle in stratified plane Couette
 842 flows. On one hand, the near-wall temperature structure (see in figure 5) is strongly
 843 Pr -dependent (as discussed in §3). Therefore, Pr has an explicit effect on the heat flux
 844 q_w through the wall (as shown in §4). This quantity is relevant for the Monin–Obukhov
 845 scalings of the interior turbulence as presented in §5. On the other hand, there is no direct
 846 impact of Pr on the interior turbulence whose self-similar characteristics are determined
 847 solely by the wall fluxes (u_τ^2 and q_w) and the buoyancy parameter ($g\alpha_V$), which is in
 848 agreement with Monin–Obukhov similarity theory and the DNS results covering a wide
 849 range of Pr .

850 Monin–Obukhov similarity theory has motivated several useful scalings which are
 851 found to be consistent with DNS results, as shown in §5. The roles of the length scales h ,
 852 L and δ_ν are highlighted through their connections to flow diagnostics such as Ri_g (which
 853 is determined by h/L) and Re_b (which is determined by L/δ_ν). It is somewhat surprising
 854 to discover an upper limit for Ri_g (or equivalently, a lower limit of $Fr_h \propto Ri_g^{-1/2}$)
 855 in stratified plane Couette flow, irrespective of the externally set boundary conditions,
 856 where the turbulence is influenced strongly by the wall fluxes. This suggests that the
 857 ‘strongly stratified regime’ in the sense described in Brethouwer *et al.* (2007) might not
 858 be realizable in this type of flows, at least under equilibrium conditions. This observation
 859 motivates the further question as to how this strongly stratified regime can be accessed
 860 ‘naturally’, i.e. without specific forcing or initial conditions.

861 Within the range of Ri_g accessible in stratified plane Couette flows, i.e. $Ri_g \lesssim 0.2$, the
 862 $\kappa_t/\nu \sim Re_b Ri_g / (1 - Ri_g)$ scaling holds for the diapycnal diffusivity as shown in §6. This
 863 reinforces the now commonly held belief that Re_b is not the only relevant parameter in
 864 describing diapycnal mixing, and in particular, we have further highlighted the role of
 865 Ri_g which has also been addressed by recent studies by Salehipour & Peltier (2015) and

866 Maffioli *et al.* (2016) (although Maffioli *et al.* (2016) used Fr_h as the parameter instead,
 867 Fr_h may be related to Ri_g). As noted by Lozovatsky & Fernando (2013) and discussed
 868 in detail in this paper in §6.3, Re_b and Ri_g may or may not be independent parameters
 869 depending on the parameter range and flow geometry. Indeed, in statistically stationary
 870 turbulent stratified plane Couette flow, we find that the characteristic mid-gap value
 871 of Ri_g is set by the prevailing properties of the turbulent flow, and is not an external
 872 parameter independently adjustable from the turbulence. This property is instrumental
 873 in explaining the variation of the turbulent flux coefficient $\Gamma \approx Ri_g/(1 - Ri_g)$. No non-
 874 monotonic mixing behaviour is observed, which we hypothesize to be due to the range of
 875 Ri_g accessible in such constant-flux layers. Moreover, our results strongly indicate that
 876 the Prandtl number Pr does not have an effect on turbulent mixing away from the walls,
 877 at least for the intermediate to large Re_b values examined, i.e. $Re_b \gtrsim 60$, as shown in
 878 figure 8.

879 In the present study, we have investigated fully developed stratified plane Couette
 880 flows for which the turbulent kinetic energy balance is, to a good approximation, in
 881 a simple local equilibrium (A3) that involves shear production, viscous dissipation
 882 and diapycnal mixing, consistently with the classical modelling assumptions of Osborn
 883 (1980) – mixing is thus not particularly ‘efficient’ with $\Gamma \leq 0.25$. Possible nonlocal and
 884 nonstationary behaviour in stratified plane Couette flows is of great interest, particularly
 885 with regard to its mixing properties, and is the topic of ongoing investigations. Finally, it
 886 is important to remember that the analysis in this paper has focused on doubly-bounded
 887 constant-flux layers with momentum and buoyancy fluxes injected through smooth
 888 boundaries. Flows in geophysical settings can be considerably more complex due to
 889 surface roughness or imposed pressure gradient, (mentioning just two examples) and
 890 such additional complexities are not captured by this investigation of stratified plane
 891 Couette flows. For example, the turbulent diffusivities may exhibit strong anisotropy
 892 in horizontal and vertical directions which needs to be treated by more sophisticated
 893 models (e.g. Sukoriansky & Galperin 2013; Tastula *et al.* 2015) than the canonical
 894 Monin–Obukhov theory.

895
 896 We thank four anonymous referees whose constructive comments have helped im-
 897 prove the paper. The EPSRC Programme Grant EP/K034529/1 entitled ‘Mathematical
 898 Underpinnings of Stratified Turbulence’ is gratefully acknowledged for supporting the
 899 research presented here. We would like to thank Dr E. Deusebio for sharing the Deusebio
 900 *et al.* (2015) data and helpful discussions on this topic. Dr M. van Reeuwijk is gratefully
 901 acknowledged for suggesting an error in an early version of the manuscript.

902 **Appendix A. Monin–Obukhov scaling: dimensional quantities**

903 *A.1. Mean shear and temperature gradient*

904 Monin–Obukhov similarity theory (see e.g. Wyngaard (2010)) suggests that the friction
 905 velocity u_τ , the wall heat flux q_w and the buoyancy parameter $g\alpha_V$ are the only relevant
 906 dimensional quantities for the dynamics of the turbulence sufficiently far away from the
 907 walls. These quantities form the similarity length scale L as defined in (1.1). According
 908 to Monin–Obukhov theory, the mean shear S and temperature gradient $d\theta/dy$ vary
 909 self-similarly with respect to the transformed wall-normal coordinate $\xi \equiv y_w/L$, i.e. the
 910 wall-normal distance y_w normalised by L . These formulae for S and $d\theta/dy$ are shown in

911 (3.11), and they can be rewritten, for simplicity, as

$$S \equiv \frac{\partial U}{\partial y} = \frac{u_\tau}{\ell_m^*} \quad \text{and} \quad \frac{\partial \Theta}{\partial y} = \frac{\theta_\tau}{\ell_s^*} = \frac{q_w/u_\tau}{\ell_s^*}, \quad (\text{A } 1)$$

912 where ℓ_m^* and ℓ_s^* are the mixing lengths for momentum and scalar respectively. The
 913 lengths ℓ_m^* and ℓ_s^* are both functions of y_w (or $\xi \equiv y_w/L$), and their closed-form
 914 expressions for the channel gap interior, following Monin–Obukhov theory, are shown
 915 in (3.13). With (A 1) and (1.1), the squared buoyancy frequency can be written as

$$N^2 \equiv g\alpha_V \frac{\partial \Theta}{\partial y} = g\alpha_V \frac{q_w/u_\tau}{\ell_s^*} = \frac{u_\tau^2}{k_m L \ell_s^*}. \quad (\text{A } 2)$$

916 A.2. Turbulent kinetic energy budget

917 Far enough away from the walls, i.e. $y^+ \equiv y_w/\delta_\nu > 50$, in fully developed turbulent
 918 stratified plane Couette flows, the balance of the turbulent kinetic energy involves shear
 919 production P , dissipation ε and buoyancy flux $B \equiv -\langle \rho'v' \rangle / (g\rho_0)$ as the dominant terms
 920 (García-Villalba *et al.* 2011*b*), i.e.

$$P \approx \varepsilon - B, \quad (\text{A } 3)$$

921 where the shear production scales as

$$P \equiv \langle u'v' \rangle S \sim u_\tau^2 S \sim \frac{u_\tau^3}{\ell_m^*}. \quad (\text{A } 4)$$

922 Invoking the definition of turbulent diffusivity κ_t via the flux-gradient relation, i.e.

$$\kappa_t \equiv -\frac{\langle \rho'v' \rangle}{d\bar{\rho}/dy}, \quad (\text{A } 5)$$

923 the buoyancy flux B can be written as $B = -\kappa_t N^2$. Following the mixing length
 924 specifications (3.6) and (3.10), as well as the expression for N^2 in (A 2), B can be rewritten
 925 as

$$B = -\ell_s^* u_\tau N^2 = -\frac{u_\tau^3}{k_m L}. \quad (\text{A } 6)$$

926 As is shown in §5, in figure 7 in particular, the flux Richardson number, defined as
 927 $Ri_f \equiv -B/P$, is typically smaller than 0.2 in stratified plane Couette flows. One may
 928 make the further approximation $-B \ll P$ in (A 3), which results in the following scaling
 929 for ε :

$$\varepsilon \approx (1 - Ri_f)P \sim P \sim \frac{u_\tau^3}{\ell_m^*}. \quad (\text{A } 7)$$

930 Appendix B. Monin–Obukhov scaling: dimensionless quantities

931 The gradient Richardson number Ri_g can be evaluated from (A 1) and (A 2):

$$Ri_g \equiv \frac{N^2}{S^2} = \frac{u_\tau^2}{k_m L \ell_s^*} \frac{\ell_m^{*2}}{u_\tau^2} = \frac{\ell_m^{*2}}{k_m L \ell_s^*}. \quad (\text{B } 1)$$

932 With ℓ_m^* and ℓ_s^* prescribed by Monin–Obukhov theory shown in (3.13), Ri_g can be written
 933 as a function of the transformed wall-normal coordinate ξ , i.e.

$$Ri_g(\xi) = \frac{k_m}{k_s} \frac{\xi^{-1} + \beta_s}{(\xi^{-1} + \beta_m)^2}, \quad (\text{B } 2)$$

934 where k_m , k_s , β_m and β_s are all dimensionless constants in Monin–Obukhov theory (§3.1).

935 We are particularly interested in the Ri_g value at $y = 0$ ($y_w = h$ or $\xi = h/L$), a
 936 location characteristic of the mid-gap plateau as shown in figure 5. Such a characteristic
 937 Ri_g value can be obtained by evaluating (B 2) at $\xi = h/L$:

$$Ri_g|_{y=0} = \frac{k_m}{k_s} \frac{(h/L)^{-1} + \beta_s}{[(h/L)^{-1} + \beta_m]^2}, \quad (\text{B } 3)$$

938 an expression that has no explicit dependence on the Prandtl number Pr . The influence of
 939 Pr on the interior Ri_g is indirect through the modulation of wall fluxes which determine
 940 the Obukhov length scale L as defined in (1.1).

941 Combining (A 2) and (A 7), one can obtain an estimate for the buoyancy Reynolds
 942 number Re_b :

$$Re_b \equiv \frac{\varepsilon}{\nu N^2} \sim \frac{u_\tau L}{\nu} \frac{\ell_s^*}{\ell_m^*} k_m = L^+ \frac{\ell_s^*}{\ell_m^*} k_m. \quad (\text{B } 4)$$

943 As discussed in §3.1, the ratio ℓ_s^*/ℓ_m^* is typically of order unity, as prescribed by Monin–
 944 Obukhov theory. The above scaling (cf. Scotti & White (2016)) thus becomes

$$Re_b \sim L^+ k_m. \quad (\text{B } 5)$$

945 Following (A 4) and (A 6), the flux Richardson number Ri_f can be estimated as

$$Ri_f \equiv \frac{-B}{P} \sim \frac{\ell_m^*}{k_m L}. \quad (\text{B } 6)$$

946 With (B 1), the above scaling becomes $Ri_f \sim (\ell_s^*/\ell_m^*) Ri_g$. Again, with ℓ_s^*/ℓ_m^* being $O(1)$,
 947 one obtains

$$Ri_f \sim Ri_g, \quad (\text{B } 7)$$

948 which is consistent with the observations of DCT (see e.g. their figure 13).

949 The other relevant parameter is the horizontal turbulent Froude number $Fr_h \equiv$
 950 $U'/(\ell_h N)$ (e.g. Billant & Chomaz (2001); Brethouwer *et al.* (2007)) which can be
 951 estimated by assuming

$$\varepsilon = \frac{U'^3}{\ell_h} \quad (\text{B } 8)$$

952 for the horizontal motions of the integral scale ℓ_h undergoing a forward cascade. Fr_h can
 953 then be estimated as (see e.g. Maffioli *et al.* (2016))

$$Fr_h \equiv \frac{U'}{\ell_h N} \sim \frac{\varepsilon}{N U'^2} \sim \frac{\varepsilon}{N u_\tau^2}, \quad (\text{B } 9)$$

954 for stratified plane Couette flows. Upon substituting (A 2) and (A 7) into (B 9), we obtain

$$Fr_h^2 \sim \frac{\varepsilon^2}{N^2 u_\tau^4} \sim \frac{u_\tau^6}{\ell_m^{*2} k_m L \ell_s^* u_\tau^4} = \frac{k_m L \ell_s^*}{\ell_m^{*2}}. \quad (\text{B } 10)$$

955 Using (B 1), one obtains a scaling for Fr_h as a function of Ri_g :

$$Fr_h \sim \frac{1}{\sqrt{Ri_g}}. \quad (\text{B } 11)$$

Appendix C. Osborn formulation for the turbulent flux coefficient

The steady-state turbulent kinetic energy balance $P \approx \varepsilon - B$ leads to

$$-B \approx \frac{Ri_f}{1 - Ri_f} \varepsilon. \quad (\text{C1})$$

Dividing the above equation by νN^2 and using $B = -\kappa_t N^2$,

$$\frac{\kappa_t}{\nu} \approx \frac{Ri_f}{1 - Ri_f} \frac{\varepsilon}{\nu N^2} = \Gamma Re_b, \quad (\text{C2})$$

where

$$\Gamma \equiv \frac{B}{\varepsilon} \approx \frac{Ri_f}{1 - Ri_f} \quad (\text{C3})$$

is the turbulent flux coefficient, and it is a fundamental question how Γ (commonly referred to as ‘mixing efficiency’ in the oceanographic literature) is to be parameterized (see e.g. Ivey *et al.* (2008)).

REFERENCES

- ARMENIO, V. & SARKAR, S. 2002 An investigation of stably stratified turbulent channel flow using large-eddy simulation. *J. Fluid Mech.* **459**, 1–42.
- BARRY, M. E., IVEY, G. N., WINTERS, K. B. & IMBERGER, J. 2001 Measurements of diapycnal diffusivities in stratified fluids. *J. Fluid Mech.* **442**, 267–291.
- BATCHELOR, G.K. 1959 Small-scale variation of convected quantities like temperature in turbulent fluid. Part 1. General discussion and the case of small conductivity. *J. Fluid Mech.* **5**, 113–133.
- BEWLEY, T. R. 2010 *Numerical Renaissance: Simulation, Optimization, and Control*. Renaissance, San Diego, California (available at <http://numerical-renaissance.com>).
- BILLANT, P. & CHOMAZ, J.-M. 2001 Self-similarity of strongly stratified inviscid flows. *Phys. Fluids* **13**, 1645–1651.
- BOUFFARD, D. & BOEGMAN, L. 2013 A diapycnal diffusivity model for stratified environmental flows. *Dyn. Atmos. Oceans* **61–62**, 14–34.
- BRADSHAW, P. & HUANG, G. P. 1995 The law of the wall in turbulent flow. *Proc. R. Soc. Lond. A* **451**, 165–188.
- BRETHOUWER, G., BILLANT, P., LINDBORG, E. & CHOMAZ, J.-M. 2007 Scaling analysis and simulation of strongly stratified turbulent flows. *J. Fluid Mech.* **585**, 343–368.
- BRITTER, R.E. 1974 An experiment on turbulence in a density stratified fluid. PhD thesis, Monash University, Victoria, Australia.
- DE BRUYN KOPS, S. M. 2015 Classical scaling and intermittency in strongly stratified boussinesq turbulence. *J. Fluid Mech.* **775**, 436–463.
- CAULFIELD, C. P. & PELTIER, W. R. 2000 The anatomy of the mixing transition in homogeneous and stratified free shear layers. *J. Fluid Mech.* **413**, 1–47.
- CAULFIELD, C. P., TANG, W. & PLASTING, S. C. 2004 Reynolds number dependence of an upper bound for the long-time-averaged buoyancy flux in plane stratified couette flow. *J. Fluid Mech.* **498**, 315–332.
- CHUNG, D. & MATHEOU, G. 2012 Direct numerical simulation of stationary homogeneous stratified sheared turbulence. *J. Fluid Mech.* **696**, 434–467.
- DAVIDSON, P. A. 2004 *Turbulence: An Introduction for Scientists and Engineers*. Oxford University Press.
- DAVIS, K. A. & MONISMITH, S. G. 2011 The modification of bottom boundary layer turbulence and mixing by internal waves shoaling on a barrier reef. *J. Phys. Oceanogr.* **41**, 2223–2241.
- DEUSEBIO, E., CAULFIELD, C. P. & TAYLOR, J. R. 2015 The intermittency boundary in stratified plane Couette flow. *J. Fluid Mech.* **781**, 298–329, referred to in the text as DCT.
- DIAMESSIS, P. J., SPEDDING, G. R. & DOMARADZKI, J. A. 2011 Similarity scaling and vorticity

- 999 structure in high-Reynolds-number stably stratified turbulent wakes. *J. Fluid Mech.* **671**,
1000 52–95.
- 1001 VAN DRIEST, E. R. 1956 On turbulent flow near a wall. *J. Aeronaut. Sci.* **23**, 1007–1011.
- 1002 EAVES, T. S. & CAULFIELD, C. P. 2015 Disruption of SSP/VWI states by a stable stratification.
1003 *J. Fluid Mech.* **784**, 548–564.
- 1004 ELLISON, T.H. 1957 Turbulent transport of heat and momentum from an infinite rough plane.
1005 *J. Fluid Mech.* **2**, 456–466.
- 1006 FERNANDO, H. J. S. 1991 Turbulent mixing in stratified fluids. *Annu. Rev. Fluid Mech.* **23**,
1007 455–493.
- 1008 FLORES, O. & RILEY, J. J. 2011 Analysis of turbulence collapse in stably stratified surface
1009 layers using direct numerical simulation. *Bound.-Lay. Meteorol.* **139**, 241–259.
- 1010 FOKEN, T. 2006 50 years of the Monin–Obukhov similarity theory. *Bound.-Lay. Meteorol.* **119**,
1011 431–447.
- 1012 GALPERIN, B., SUKORIANSKY, S. & ANDERSON, P. S. 2007 On the critical richardson number
1013 in stably stratified turbulence. *Atmos. Sci. Lett.* **8**, 65–69.
- 1014 GARCÍA-VILLALBA, M. & DEL ÁLAMO, J. C. 2011 Turbulence modification by stable
1015 stratification in channel flow. *Phys. Fluids* **23**, 045104.
- 1016 GARCÍA-VILLALBA, M., AZAGRA, E. & UHLMANN, M. 2011a A numerical study of turbulent
1017 stably-stratified plane Couette flow. In *High Performance Computing in Science and*
1018 *Engineering '10* (ed. W. E. Nagel *et al.*), pp. 251–261. Springer-Verlag.
- 1019 GARCÍA-VILLALBA, M., AZAGRA, E. & UHLMANN, M. 2011b Mixing efficiency in stably-
1020 stratified plane Couette flow. In *Proceedings of the 7th Int. Symp. on Stratified Flows,*
1021 *Rome, Italy.*
- 1022 HOLFORD, J. M. & LINDEN, P. F. 1999 Turbulent mixing in a stratified fluid. *Dynam. Atmos.*
1023 *Oceans* **30**, 173–198.
- 1024 HOWARD, L. N. 1961 Note on a paper of John W. Miles. *J. Fluid Mech.* **10**, 509–512.
- 1025 IVEY, G. N., WINTERS, K. B. & KOSEFF, J. R. 2008 Density stratification, turbulence, but
1026 how much mixing? *Annu. Rev. Fluid Mech.* **40**, 169.
- 1027 KARIMPOUR, F. & VENAYAGAMOORTHY, S. K. 2014 A simple turbulence model for stably
1028 stratified wall-bounded flows. *J. Geophys. Res.* **119**, 870–880.
- 1029 KARIMPOUR, F. & VENAYAGAMOORTHY, S. K. 2015 On turbulent mixing in stably stratified
1030 wall-bounded flows. *Phys. Fluids* **27**, 046603.
- 1031 LILLY, D. K. 1983 Stratified turbulence and the mesoscale variability of the atmosphere. *J.*
1032 *Atmos. Sci.* **40**, 749–761.
- 1033 LINDEN, P. F. 1979 Mixing in stratified fluids. *Geophys. Astro. Fluid Dyn.* **13**, 3–23.
- 1034 LINDEN, P. F. 1980 Mixing across a density interface produced by grid turbulence. *J. Fluid*
1035 *Mech.* **100**, 691–703.
- 1036 LOZOVATSKY, I. D. & FERNANDO, H. J. S. 2013 Mixing efficiency in natural flows. *Phil. Trans.*
1037 *R. Soc. A* **371**, 20120213.
- 1038 MAFFIOLI, A., BRETTHOUWER, G. & LINDBORG, E. 2016 Mixing efficiency in stratified
1039 turbulence. *J. Fluid Mech.* **794**, R3.
- 1040 MAFFIOLI, A. & DAVIDSON, P. A. 2015 Dynamics of stratified turbulence decaying from a high
1041 buoyancy reynolds number. *J. Fluid Mech.* **786**, 210–233.
- 1042 MAHRT, L. 1999 Stratified atmospheric boundary layers. *Bound.-Lay. Meteorol.* **90**, 375–396.
- 1043 MAHRT, L. 2014 Stably stratified atmospheric boundary layers. *Annu. Rev. Fluid Mech.* **46**,
1044 23–45.
- 1045 MASHAYEK, A., CAULFIELD, C. P. & PELTIER, W. R. 2013 Time-dependent, non-monotonic
1046 mixing in stratified turbulent shear flows: Implications for oceanographic estimates of
1047 buoyancy flux. *J. Fluid Mech.* **736**, 570–593.
- 1048 MATER, B. D. & VENAYAGAMOORTHY, S. K. 2014 The quest for an unambiguous
1049 parameterization of mixing efficiency in stably stratified geophysical flows. *Geophys. Res.*
1050 *Lett.* **41**, 4646–4653.
- 1051 MILES, J. W. 1961 On the stability of heterogeneous shear flows. *J. Fluid Mech.* **10**, 496–508.
- 1052 OGLETHORPE, R. L. F., CAULFIELD, C. P. & WOODS, A. W. 2013 Spontaneous layering in
1053 stratified turbulent Taylor–Couette flow. *J. Fluid Mech.* **721**, R3.

- 1054 OSBORN, T. R. 1980 Estimates of the local rate of vertical diffusion from dissipation
1055 measurements. *J. Phys. Oceanogr.* **10**, 83–89.
- 1056 PARK, Y. G., WHITEHEAD, J. A. & GNANADESKIAN, A. 1994 Turbulent mixing in stratified
1057 fluids: layer formation and energetics. *J. Fluid Mech.* **279**, 279–311.
- 1058 PELTIER, W. R. & CAULFIELD, C. P. 2003 Mixing efficiency in stratified shear flows. *Annu.*
1059 *Rev. Fluid Mech.* **35**, 135–167.
- 1060 PHAM, H. T., SARKAR, S. & WINTERS, K. B. 2013 Large-eddy simulation of deep-cycle
1061 turbulence in an Equatorial Undercurrent model. *J. Phys. Oceanogr.* **43**, 2490–2502.
- 1062 PHILLIPS, O. M. 1972 Turbulence in a strongly stratified fluid – is it unstable? *Deep-Sea Res.*
1063 **19**, 79–81.
- 1064 POPE, S. B. 2000 *Turbulent Flows*. Cambridge University Press.
- 1065 VAN REEUWIJK, M. & HADŽIABDIĆ, M. 2015 Modelling high schmidt number turbulent mass
1066 transfer. *Int. J. Heat Fluid Fl.* **51**, 42–49.
- 1067 RILEY, J. J. & DE BRUYN KOPS, S. M. 2003 Dynamics of turbulence strongly influenced by
1068 buoyancy. *Phys. Fluids* **15**, 2047.
- 1069 RILEY, J. J. & LINDBORG, E. 2012 Recent progress in stratified turbulence. In *Ten Chapters in*
1070 *Turbulence* (ed. P. A. Davidson, Y. Kaneda & K. R. Sreenivasan), pp. 269–317. Cambridge
1071 University Press.
- 1072 ROHR, J. & VAN ATTA, C. 1987 Mixing efficiency in stably stratified growing turbulence. *J.*
1073 *Geophys. Res.* **92**, 5481–5488.
- 1074 SALEHIPOUR, H., CAULFIELD, C. P. & PELTIER, W. R. 2016 Turbulent mixing due to the
1075 Holmboe wave instability at high Reynolds number. *J. Fluid Mech.* **803**, 591–621.
- 1076 SALEHIPOUR, H., PELTIER, W. R. & MASHAYEK, A. 2015 Turbulent diapycnal mixing in
1077 stratified shear flows: the influence of Prandtl number on mixing efficiency and transition
1078 at high Reynolds number. *J. Fluid Mech.* **773**, 178–223.
- 1079 SALEHIPOUR, H. & PELTIER, W. R. 2015 Diapycnal diffusivity, turbulent Prandtl number and
1080 mixing efficiency in Boussinesq stratified turbulence. *J. Fluid Mech.* **775**, 464–500.
- 1081 SCHLICHTING, H. & GERSTEN, K. 2003 *Boundary-Layer Theory*. Springer.
- 1082 SCOTTI, A. 2015 Biases in Thorpe-scale estimates of turbulence dissipation. Part II: Energetics
1083 arguments and turbulence simulations. *J. Geophys. Res.* **45**, 2522–2543.
- 1084 SCOTTI, A. & WHITE, B. 2016 The mixing efficiency of stratified turbulent boundary layers. *J.*
1085 *Phys. Oceanogr.* **46**, 3181–3191.
- 1086 SHIH, L. H., KOSEFF, J. R., FERZIGER, J. H. & REHMANN, C. R. 2000 Scaling and
1087 parameterization of stratified homogeneous turbulent shear flow. *J. Fluid Mech.* **412**,
1088 1–20.
- 1089 SHIH, L. H., KOSEFF, J. R., IVEY, G. N. & FERZIGER, J. H. 2005 Parameterization of turbulent
1090 fluxes and scales using homogeneous sheared stably stratified turbulence simulations. *J.*
1091 *Fluid Mech.* **525**, 193–214.
- 1092 SMYTH, W. D. & MOUM, J. N. 2013 Marginal instability and deep cycle turbulence in the
1093 eastern equatorial Pacific Ocean. *Geophys. Res. Lett.* **40**, 6181–6185.
- 1094 SMYTH, W. D., MOUM, J. N. & CALDWELL, D. R. 2001 The efficiency of mixing in turbulent
1095 patches: Inferences from direct simulations and microstructure observations. *J. Phys.*
1096 *Oceanogr.* **31**, 1969–1992.
- 1097 SUKORIANSKY, S. & GALPERIN, B. 2013 An analytical theory of the buoyancy–Kolmogorov
1098 subrange transition in turbulent flows with stable stratification. *Phil. Trans. R. Soc. A*
1099 **371**, 20120212.
- 1100 TANG, W., CAULFIELD, C. P. & KERSWELL, R. R. 2009 A prediction for the optimal
1101 stratification for turbulent mixing. *J. Fluid Mech.* **634**, 487–497.
- 1102 TASTULA, E.-M., GALPERIN, B., SUKORIANSKY, S., LUHAR, A. & ANDERSON, P. 2015 The
1103 importance of surface layer parameterization in modeling of stable atmospheric boundary
1104 layers. *Atmos. Sci. Lett.* **16**, 83–88.
- 1105 TAYLOR, J. R. 2008 *Numerical Simulations of the Stratified Oceanic Bottom Boundary Layer*.
1106 PhD thesis, University of California, San Diego.
- 1107 TAYLOR, J. R., SARKAR, S. & ARMENIO, V. 2005 Large eddy simulation of stably stratified
1108 open channel flow. *Phys. Fluids* **17**, 116602.
- 1109 THORPE, S. A. & LIU, Z. 2009 Marginal instability? *J. Phys. Oceanogr.* **39**, 2373–2381.
- 1110 TURNER, J. S. 1973 *Buoyancy Effects in Fluids*. Cambridge University Press.

- 1111 VENAYAGAMOORTHY, S. K. & STRETCH, D. D. 2010 On the turbulent Prandtl number in
1112 homogeneous stably stratified turbulence. *J. Fluid Mech.* **644**, 359–369.
- 1113 WALTER, R. K., SQUIBB, M. E., WOODSON, C. B., KOSEFF, J. R. & MONISMITH, S. G.
1114 2014 Stratified turbulence in the nearshore coastal ocean: Dynamics and evolution in the
1115 presence of internal bores. *J. Phys. Oceanogr.* **119**, 8709–8730.
- 1116 WELLS, M., CENEDESE, C. & CAULFIELD, C. P. 2010 The relationship between flux coefficient
1117 and entrainment ratio in density currents. *J. Phys. Oceanogr.* **40**, 2713–2727.
- 1118 WILSON, J. M. & VENAYAGAMOORTHY, S. K. 2015 A shear-based parameterization of turbulent
1119 mixing in the stable atmospheric boundary layer. *J. Atmos. Sci.* **72**, 1713–1726.
- 1120 WYNGAARD, J. C. 2010 *Turbulence in the Atmosphere*. Cambridge University Press.
- 1121 ZHOU, Q. 2015 Far-field evolution of turbulence-emitted internal waves and Reynolds number
1122 effects on a localized stratified turbulent flow. PhD thesis, Cornell University, Ithaca, New
1123 York.